The Effect of Arctic Freshwater Pathways on North Atlantic Convection and the Atlantic Meridional Overturning Circulation

HE WANG

Scripps Institution of Oceanography, University of California, San Diego, La Jolla, California

SONYA LEGG

Program in Atmospheric and Oceanic Sciences, Princeton University, Princeton, New Jersey

ROBERT HALLBERG

NOAA/Geophysical Fluid Dynamics Laboratory, Princeton, New Jersey

(Manuscript received 21 September 2017, in final form 30 March 2018)

ABSTRACT

This study examines the relative roles of the Arctic freshwater exported via different pathways on deep convection in the North Atlantic and the Atlantic meridional overturning circulation (AMOC). Deep water feeding the lower branch of the AMOC is formed in several North Atlantic marginal seas, including the Labrador Sea, Irminger Sea, and the Nordic seas, where deep convection can potentially be inhibited by surface freshwater exported from the Arctic. The sensitivity of the AMOC and North Atlantic to two major freshwater pathways on either side of Greenland is studied using numerical experiments. Freshwater export is rerouted in global coupled climate models by blocking and expanding the channels along the two routes. The sensitivity experiments are performed in two sets of models (CM2G and CM2M) with different control simulation climatology for comparison. Freshwater via the route east of Greenland is found to have a larger direct impact on Labrador Sea convection. In response to the changes of freshwater route, North Atlantic convection outside of the Labrador Sea changes in the opposite sense to the Labrador Sea. The response of the AMOC is found to be sensitive to both the model formulation and mean-state climate.

1. Introduction

Open-ocean deep convection in the Labrador Sea is a key contribution to the Atlantic meridional overturning circulation (AMOC), which transports about 1 PW heat to the North Atlantic (Ganachaud and Wunsch 2000). Along with the Nordic seas and Irminger Sea, the Labrador Sea supplies dense water to the AMOC's sinking branch and controls the AMOC's strength (Kuhlbrodt et al. 2007). Thus, the magnitude and stability of the Labrador Sea convection is important to the strength of the AMOC and North Atlantic climate.

Deep convection in the Labrador Sea depends on preconditioned near-surface weak stratification, which facilitates heat loss to the atmosphere during winter (Marshall and Schott 1999). Enhanced surface stratification can therefore potentially inhibit Labrador Sea open-ocean convection. Several events of reduced convection in the Labrador Sea have been recorded, associated with reduced sea surface salinity, such as the Great Salinity Anomalies (Dickson et al. 1988; Belkin et al. 1998; Belkin 2004). Recently, observations have shown an increased trend of deep convection in the Labrador Sea, with cooler and saltier deep-water formation after 2012, following a decade-long decreasing trend that started in the 1990s (Yashayaev and Loder 2017). The changes in Labrador Sea convection are suggested to be in phase with the North Atlantic Oscillation, indicating the importance of atmospheric forcing (Yashayaev 2007; Yeager and Danabasoglu 2014; Yashayaev and Loder 2017).

The large-scale impact of freshwater on convection in the Labrador Sea and other regions in the North

Denotes content that is immediately available upon publication as open access.

Corresponding author: He Wang, hew030@ucsd.edu

DOI: 10.1175/JCLI-D-17-0629.1

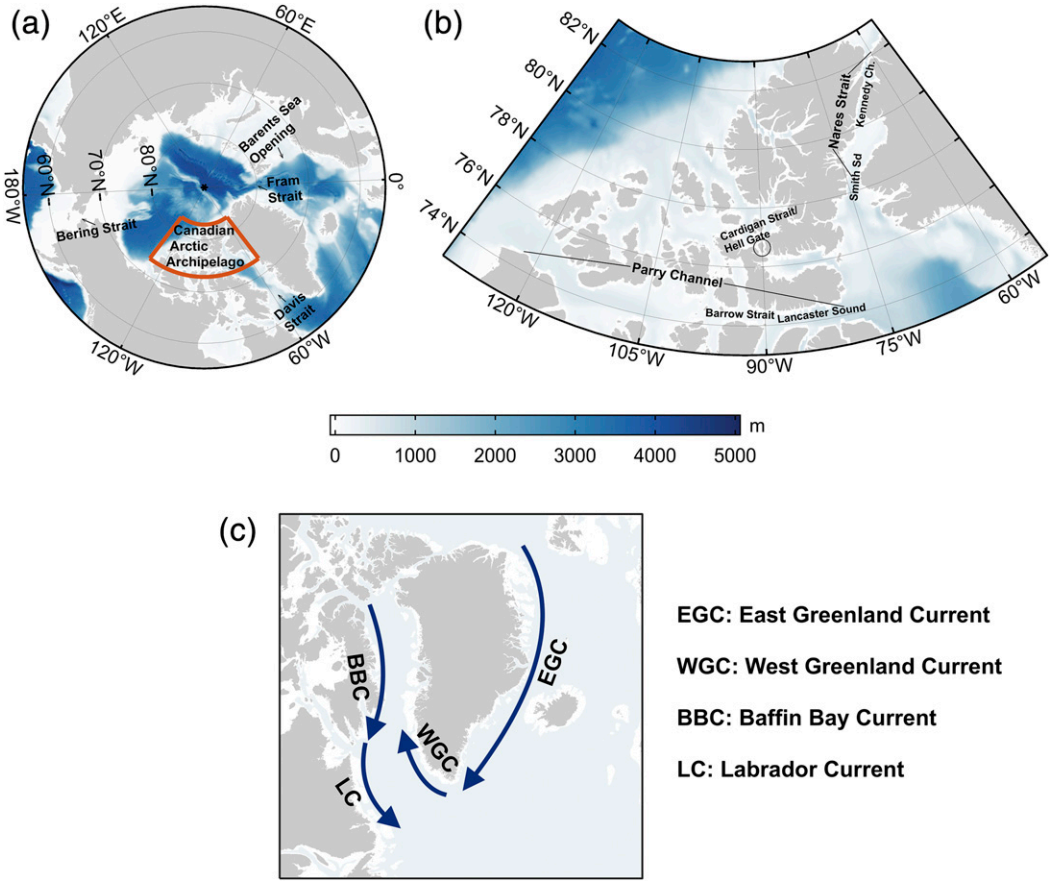

FIG. 1. Topography in the (a) Arctic and (b) CAA region from observations (ETOPO2 2 min). Panel (b) is a zoomed-in view of the red box in (a). (c) A schematic of the Arctic freshwater pathways into the Labrador Sea. Ocean deeper than 250 m is shown in light blue. Channels and waterways related to the current study are labeled in panels (a) and (b).

Atlantic has been evaluated in previous studies. Water-hosing experiments in numerical models (Manabe and Stouffer 1995; Stouffer et al. 2006; Spence et al. 2008; Jackson et al. 2015) suggest significant AMOC reduction and North Atlantic cooling in response to the weakened convection caused by the additional surface freshwater. While the reduction of the AMOC strength is not very sensitive to the location of additional freshwater input, the regional climate response varies depending on the location of the freshwater anomaly (Saenko et al. 2007; Smith and Gregory 2009; Roche et al. 2010; Liu et al. 2018). In particular, Saenko et al. (2007) found that when the freshwater anomaly is constrained along the Labrador Sea coast, the subpolar gyre becomes stronger and the western North Atlantic becomes warmer, despite cooling in other parts of the North Atlantic caused by the reduced AMOC.

The Arctic is a major source of the freshwater entering the Labrador Sea, and it enters via several different gateways (Fig. 1), including the Barents Sea and Fram Strait via the Nordic seas, and pathways through the Canadian Arctic Archipelago (CAA). From these gateways, the Arctic freshwater follows two routes to the Labrador Sea: the eastern route including freshwater mostly from Fram Strait and some from Barents Sea, and the western route via the CAA.

Eastern-route freshwater follows the southward East Greenland Current (EGC) along the east coast of Greenland to Cape Farewell, where it turns northward and enters the Labrador Sea via the West Greenland Current (WGC). Western-route freshwater passes through the CAA and Baffin Bay, then enters the Labrador Sea through the Davis Strait via the Labrador Current (LC). The western route is much shorter, and has less interaction with warm, salty Atlantic water (Fig. 1c). The CAA channels (Fig. 1b), including Parry Channel, Cardigan Strait/Hell Gate, and Nares Strait, are much shallower and narrower than the eastern route

TABLE 1. Depth-integrated volume (Sv) and freshwater (mSv) transport through all Arctic gateways in all experiments. For each gateway, total volume transport is shown in the left column, and liquid and solid freshwater transports are shown in the center and right columns, respectively. Liquid (oceanic) freshwater transport is calculated following Talley (2008): $T_{\mathrm{fresh}} = \int (v - vS/S_0)\, dldz$, where v is the velocity normal to the section, S is the salinity at the section, and S_0 is a reference salinity of 34.80 in all cases. For solid (ice) freshwater transport, a salinity of 4 psu and an ice density of 900 kg m^{-3} (as in Haine et al. 2015) are used. For the North Atlantic gateways (CAA channels, Fram Strait, and Barents Sea opening), positive values means transport into the North Atlantic. Signs of Bering Strait and Arctic precipitation minus evaporation plus river runoffs ($P - E + R$) are positive for transport into the Arctic. For experiments CONTROL_G, CONTROL_M, CLOSED_BE_G, and CLOSED_BE_M, the numbers (in bold) show their actual transports. For the remaining sensitivity experiments, the numbers (in italic) show their changes relative to the corresponding baseline experiments. The observed volume and freshwater transport of CAA channels are cited from Prinsenberg et al. (2009), Melling et al. (2008), Peterson et al. (2012), and Haine et al. (2015). Of the total freshwater transport, 48 mSv is contributed by Lancaster Sound and a slightly smaller amount from Nares Strait. Observations from Cardigan Strait/Hell Gate are not available, but the volume transport is less than half of the other two channels (Melling et al. 2008; Haine et al. 2015). Fram Strait volume transport is from Marnela et al. (2016). Fram Strait, Barents Sea opening freshwater transports, and Arctic $P - E + R$ are from Haine et al. (2015). Bering Strait transports are from Woodgate et al. (2012) and Haine et al. (2015).

	CAA channels			Fram Strait			Barents Sea			Bering Strait			Arctic
Observations	**1.4**	**96**	**1.5–2.5**	**0.8 ± 1.5**	**88 ± 13**	**60 ± 9**	**—**	**3 ± 3**	**—**	**1.1**	**79 ± 3**	**4 ± 1**	**0.2 ± 0.02**
CONTROL_G	**1.11**	**85**	**0**	**2.71**	**58**	**30**	**−2.65**	**101**	**0**	**1.02**	**91**	**1**	**0.15**
CLOSED_CAA_G	*−1.11*	*−85*	*+0*	*+0.79*	*+52*	*+11*	*+0.27*	*−12*	*+1*	*−0.01*	*−3*	*+0*	*−0.04*
WIDE_CAA_G	*+1.07*	*+34*	*+3*	*−0.85*	*−31*	*−6*	*−0.22*	*−17*	*−0*	*+0.02*	*+1*	*−0*	*−0.01*
CLOSED_FS_G	*+0.87*	*+72*	*+0*	*−2.50*	*−47*	*+4*	*+1.49*	*−33*	*+7*	*−0.15*	*−11*	*−0*	*+0.00*
CLOSED_BE_G	**0.89**	**51**	**0**	**2.38**	**16**	**19**	**−3.13**	**81**	**0**	**0.00**	**0**	**2**	**0.15**
CLOSED_BE_CAA_G	*−0.89*	*−51*	*+0*	*+0.63*	*+29*	*+6*	*+0.24*	*−4*	*+0*	*0.00*	*0*	*+0*	*−0.02*
CONTROL_M	**0.43**	**15**	**1**	**3.17**	**20**	**45**	**−2.44**	**114**	**1**	**1.05**	**44**	**2**	**0.11**
CLOSED_CAA_M	*−0.43*	*−15*	*−1*	*+0.39*	*+17*	*+2*	*+0.05*	*−4*	*+0*	*+0.01*	*+0*	*+0*	*−0.00*
WIDE_CAA_M	*+1.88*	*+10*	*+4*	*−1.26*	*−30*	*−9*	*−0.58*	*+26*	*−0*	*+0.03*	*+0*	*+0*	*+0.01*
CLOSED_BE_M	**0.54**	**5**	**1**	**3.17**	**−65**	**30**	**−3.59**	**173**	**0**	**0.00**	**0**	**0**	**0.12**
CLOSED_BE_CAA_M	*−0.54*	*−5*	*−1*	*+0.37*	*+18*	*+3*	*+0.17*	*−11*	*+0*	*0.00*	*0*	*0*	*+0.00*

through Fram Strait, but they allow only slightly less freshwater export through the western [>96 mSv (1 Sv ≡ 10^6 m^3 s^{-1}); Münchow et al. 2006; Prinsenberg and Hamilton 2005; Dickson et al. 2007; Melling et al. 2008; Prinsenberg et al. 2009; Peterson et al. 2012] compared with the eastern pathways (150 mSv; Aagaard and Carmack 1989; Dickson et al. 2007; Peterson et al. 2012; Haine et al. 2015; Table 1).

In addition to the Arctic, the Greenland ice sheet provides another source of freshwater into the Labrador Sea (Yang et al. 2016). Previous studies (e.g., Velicogna et al. 2014) have shown an increased rate of Greenland ice melting. The same climate models as are used in this paper demonstrate a sensitivity of the AMOC response to the spatial distribution of Greenland meltwater discharge on time scales of a few centuries, but less sensitivity on longer time scales after the freshwater has been distributed throughout the subpolar Atlantic (Liu et al. 2018).

Previous studies provide conflicting views of the responses of Labrador Sea convection and the AMOC to the freshwater inflow via the western and eastern routes. Wadley and Bigg (2002) found Labrador Sea convection and the AMOC are enhanced in response to a closed CAA in an ocean-only model. Komuro and Hasumi (2005) found the opposite response in experiments with both a widely opened and closed CAA in a forced ocean and sea ice model with a higher resolution. They report both stronger Labrador Sea convection and AMOC strength in the case with a widely opened CAA and stronger freshwater inflow via the western route, suggesting that freshwater via Fram Strait (i.e., following the eastern route) has a larger influence on the deep-water formation in the North Atlantic. This conclusion is supported by Myers (2005), who uses an eddy-permitting model to show that freshwater following the LC is less able to reduce the convection compared with the eddy-rich WGC. The role of WGC eddies on Labrador Sea restratification is indicated in modeling (Eden and Böning 2002; Kawasaki and Hasumi 2014; Saenko et al. 2014) and observational studies (Schmidt and Send 2007; Hátún et al. 2007; Myers et al. 2009), while the influence of LC remains under debate.

In addition to conflicting opinions of the relative roles of freshwater from eastern/western routes, the sensitivity of the AMOC to variability in the freshwater pathways is not fully understood. In particular, changes in freshwater routes to the Labrador Sea inevitably involve changes in other convective regions of the North Atlantic. For example, Wadley and Bigg (2002) showed that Nordic sea convection experiences changes of the opposite sign to the Labrador Sea.

Recently, Otto-Bliesner et al. (2017) investigated the effect of a closed CAA during the Pliocene using climate models with reconstructed Pliocene boundary conditions, during which time the atmospheric radiative forcing was at about the same level as today, but the Bering Strait was closed. They found that a closed Bering Strait results in a strengthened AMOC, and a closed CAA leads to a weakened AMOC. The combination of the two leads to an even stronger AMOC, which suggests that altering Arctic freshwater export pathways may lead to different responses of the AMOC depending on the status of the Bering Strait.

Here, we use two state-of-the-art coupled models to further address the question of the roles Arctic freshwater routes play in Labrador Sea convection and the AMOC. Specifically, we test the relative impacts of freshwater via the eastern and western routes on all North Atlantic convectively active regions, and evaluate the response of the AMOC to changes in North Atlantic convection. While the models we use have similar climatology in many aspects, they differ in their Arctic/Subarctic circulation and freshwater exports via the CAA and Fram Strait. Similarities and differences between the two models indicate the sensitivity of the AMOC's response to mean-state climate. We find that in both models, the eastern route generally has a stronger impact on Labrador Sea convection. Changes in freshwater route also impact convection in other regions, which tends to compensate the changes in the Labrador Sea. The influence on the total deep-water formation and the AMOC depends on the model details and mean-state climate.

2. Model descriptions

The models we use here are Geophysical Fluid Dynamics Laboratory (GFDL)'s coupled physical climate models CM2G and CM2M, the non-biogeochemistry/carbon cycle versions of the CMIP5 ESM2G and ESM2M (Dunne et al. 2012). CM2G and CM2M use identical atmosphere (AM2), sea ice (SIS), and land (LM3) models. CM2M is very similar to the previous GFDL coupled model CM2.1 (Delworth et al. 2006), with a newer version of the land model and ocean model (Dunne et al. 2012). The radiative forcing adopted in both models is at the year 1990 level.

The only different component between CM2G and CM2M is the ocean model. CM2G uses the isopycnal model Generalized Ocean Layer Dynamics (GOLD; Hallberg and Adcroft 2009) as its ocean component. In GOLD, a 1° Mercator resolution is used in the horizontal (with finer resolution up to 0.33° at the equator), discretized on a C-grid. In the vertical, GOLD has 63 σ_2 (potential density referenced to 2000 dbar) layers, with two mixed layers and two buffer layers as the first four layers. CM2M uses the Modular Ocean Model (MOM, version 4p1; Griffies 2009) with 50 geopotential levels in the vertical and a similar horizontal 1° resolution as in GOLD with a B-grid discretization. Performances of the Earth system model versions as well as a comparison of the two models are evaluated in Dunne et al. (2012).

In this study, both models have a simulation length of centuries (700 years for CM2M and 1000 years for CM2G) after initialization, allowing the deep-ocean circulation to reach a relatively steady state. Note that all components except for the ocean model are tuned to ensure an optimized performance of CM2M. For a clean comparison of the impact of the ocean model formulation, these respective models are not retuned in CM2G, resulting in a longer time for CM2G to reach steady state and some inherent mean-state biases.

CM2G can represent channels with widths smaller than the resolved grid size (Adcroft 2013). For the three CAA pathways, realistic widths of the channels are adopted at their narrowest parts (Fig. 2a) at Kennedy Channel (of Nares Strait, 38.0 km) and Cardigan Strait/Hell Gate (8.4 km), but not at Parry Channel, where the grid cell width (32.9 km) at its narrowest part in the model (Lancaster Sound) is narrower than the real channel width.

There is no similar treatment for subgrid-scale channel width in CM2M, and the CM2M B-grid requires at least two ocean grid cells to allow flow through a channel. Thus, CAA channels in CM2M are much wider than in CM2G, as shown in Fig. 2b.[1]

3. Control simulations

a. Mean state

1) The AMOC and North Atlantic convection

The AMOC volume transport in CM2M is much stronger than in CM2G. Averaged over the last 200 years of simulation, the maximum AMOC streamfunction at 49°N is 22.5 Sv in CM2G and 26.6 Sv in CM2M [for a more detailed comparison of the AMOC volume transport and streamfunctions, see Wang et al. (2015)]. Both AMOC transport magnitudes are larger

[1] Specifically, Cardigan Strait/Hell Gate is too narrow to be resolved; Nares Strait at Smith Sound (southwest of Kennedy Channel) has a width of 190.3 km and Parry Channel at Barrow Strait (west of Lancaster Sound) is 65.9 km wide, resulting in a wider total opening compared with CM2G.

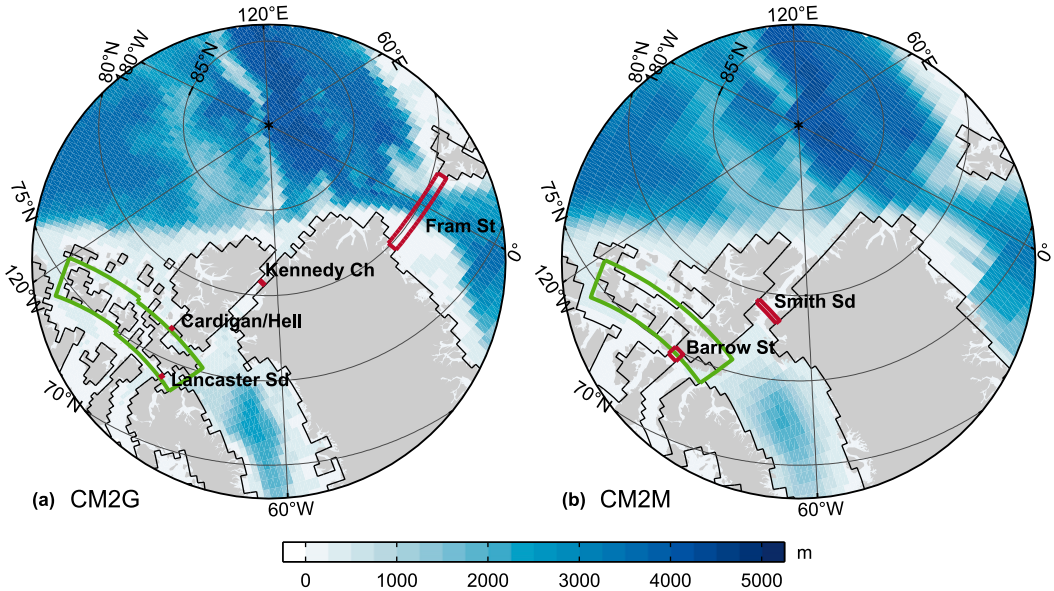

FIG. 2. Experiment design shown on model topography (shaded color) maps in (a) CM2G and (b) CM2M. Real-world land is denoted by shaded gray color, and locations of model coastlines are superimposed as black lines. Red boxes and lines show blocked channels for closed CAA channels and closed Fram Strait experiments, where lines mean channel widths are defined as zero and boxes denote lifted topography. Green boxes denote removed islands and deepened ocean for widened CAA channel experiments.

than the observationally based estimate of 18 Sv from Talley et al. (2003), and inverse model estimate of 16.3 ± 2.7 Sv from Lumpkin and Speer (2007) at the same latitude. At 26°N, transports are also stronger than the Rapid Climate Change (RAPID) observationally based estimate (18.5 Sv; Johns et al. 2011) for both CM2G (21.3 Sv) and CM2M (21.9 Sv).

The difference in AMOC strength results from the differences in the North Atlantic deep-water formation, which is illustrated in mixed layer depth (MLD) in Fig. 3.[2] Compared with the observations, convection in both models tends to have biases in geographic distribution and relative strength. In CM2M, convection in the Nordic seas is too weak (relative to other regions) and geographically restrained; Labrador Sea convection, on the other hand, is overly strong and extends too far south. In CM2G, MLD in the Nordic seas is too deep and convection extends too far to the southeast. In the Irminger Sea, where deep-convection events have also been observed, CM2G shows a relative strong convection, while that in CM2M is weaker.

2) DECOMPOSITION OF THE NADW

To quantify the contribution from different deep-water formation regions to the AMOC, we decompose the zonally integrated southward North Atlantic Deep Water (NADW) transport into dense water transport from the north (with the major contribution from the Nordic seas overflows) and diapycnal transport within the North Atlantic box region (Fig. 4). Assuming steady state (averaged over the last 200 years), the downward diapycnal transport through a certain isopycnal in a box region can be calculated as the residual of the net transport through the boundaries. The isopycnal σ_2 = 36.79 kg m^{-3} is used for CM2G and σ_2 = 36.63 kg m^{-3} is used for CM2M, which is the isopycnal where the zonally integrated meridional transport switches directions at 49°N, and the AMOC reaches its maximum transport in density space.

[2] CM2G and CM2M apply different methods for the surface boundary layer dynamics: CM2G uses a parameterization based on bulk energetics (Kraus and Turner 1967; Hallberg 2003) and CM2M uses K-profile parameterization (Large et al. 1994). Thus the diagnostics of MLD in the two models have different meanings. In CM2G, MLD is the thickness of the depth of active turbulence. In CM2M, MLD is measured as the depth of a buoyancy decrease relative to the surface. Strictly speaking, the two MLDs cannot be directly compared with each other and with observational data here. (A more standard practice for intermodel MLD comparison is to calculate MLD offline using hydrological profiles based on a common definition. Unfortunately, this could not be done since monthly temperature and salinity data were not saved; only annual means were saved.) Nonetheless, comparison of relative strength of MLD in different regions within one model and changes of MLD in perturbation experiments can still be made and will be used as a measure of the convection strength through this paper.

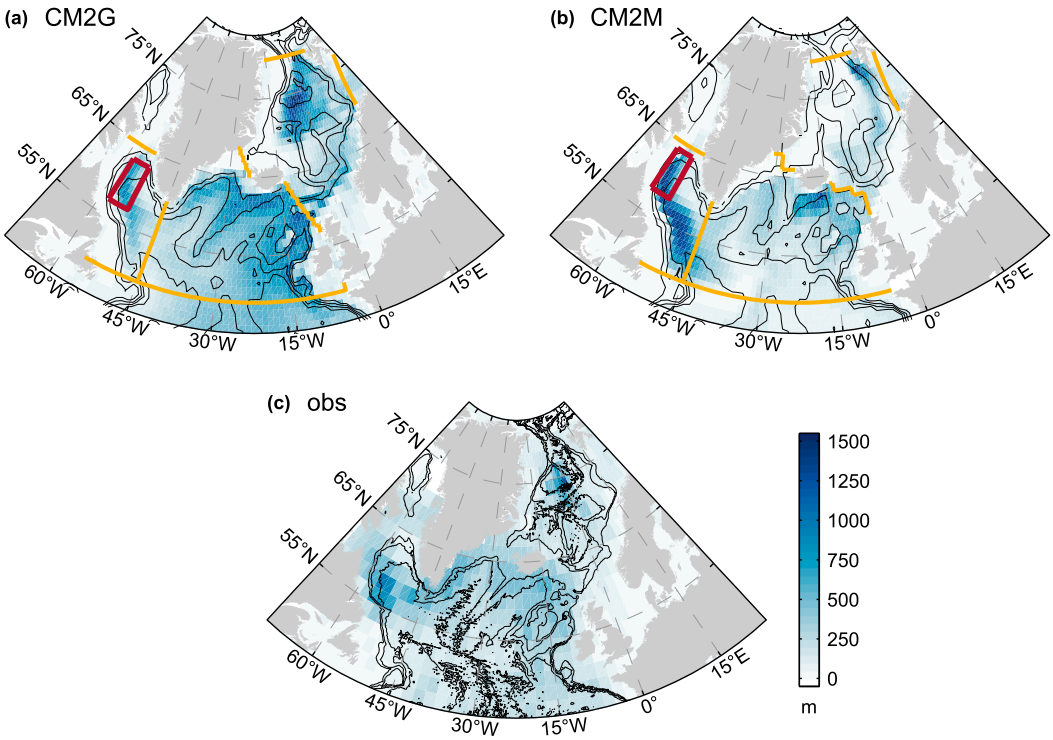

FIG. 3. Time-averaged March MLD in (a) CM2G, (b) CM2M, and (c) observations. Observation data is from de Boyer Montégut et al. (2004). Thin black contour lines show the topography referenced to the sea level with an interval of 1000 m. Observed topography is from ETOPO2 2-min data. The red boxes in the Labrador Sea denote regions of averaged MLD index used in Fig. 5. The yellow lines denote the boundaries used for transport budget calculation in Fig. 4 and area-integrated diapycnal transports in Fig. 7.

The diapycnal transport contributes to the majority of the southward deep-water transport in both models. CM2G has a larger contribution than CM2M from the Nordic seas overflow water.[3] The differences in Labrador Sea convection between the two models are not reflected in this diagnostic, as the transformation in the Labrador Sea happens at a denser level than the isopycnal surface used here. Outside of the Labrador Sea, CM2M has a much larger diapycnal transport than CM2G, compensating for its smaller overflow transport and resulting in a stronger total NADW transport and AMOC than CM2G.

b. *The AMOC and Labrador Sea convection*

As an important component of the source water of the NADW, variability of Labrador Sea convection influences that of the AMOC in both models. Time series of the AMOC and Labrador Sea March MLD from the multicentury simulations are shown in Figs. 5a and 5b.

In addition to a stronger time-mean transport, the AMOC in CM2M also has a strong decadal variability. Large-amplitude fluctuations are also seen in CM2M's Labrador Sea MLD, which are associated with the strong variability in the AMOC. By contrast, multidecadal variability of the AMOC and Labrador Sea MLD in CM2G is much weaker (see also Dunne et al. 2012).

In CM2G, there are two events of sharp decrease of Labrador Sea MLD around model year 2600 and year 2800, and both are associated with reductions of the AMOC transport. These events could be seen as the model counterparts of the Great Salinity Anomaly events. These two events with significantly reduced MLD are accompanied by fresh anomalies near the surface (Figs. 6a,c,e), which leads to strengthened surface stratification. By contrast, relatively regular multidecadal fluctuations of temperature and salinity anomalies are prominent in the CM2M profiles (Figs. 6b,d,f), and most of the periods with freshwater-capped Labrador Sea are shorter than the two events in CM2G. Also, note that the temperature and salinity fluctuations in CM2M reach a greater depth than in CM2G; this is possibly associated with the differences in

[3] The overflow transport is calculated using a density criterion; the readers are referred to Wang et al. (2015) for details of the choices of the isopycnals in both CM2G and CM2M.

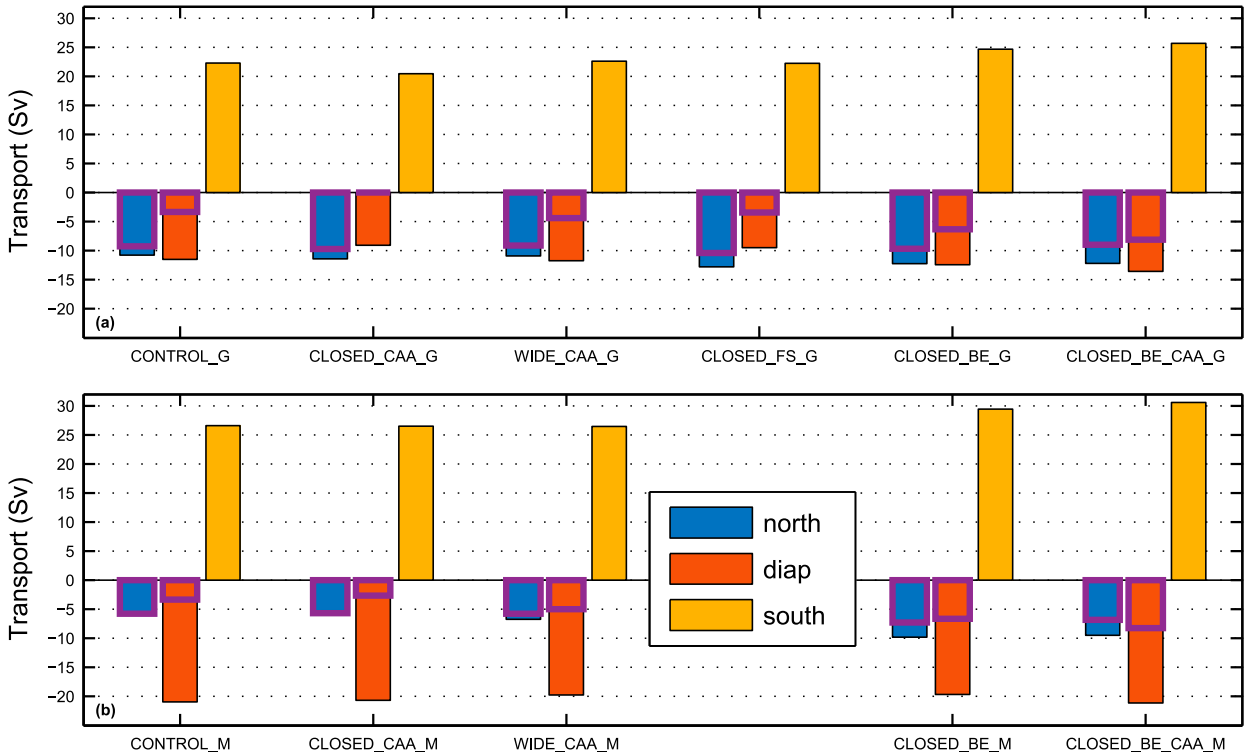

FIG. 4. Transport budget in the North Atlantic box (bounded by the yellow lines south of the GIS ridge in Fig. 3) for all (upper panel) CM2G and (lower panel) CM2M experiments listed in Table 2.The box is bounded by Davis Strait and the GIS ridge in the north, 49°N in the south, and an isopycnal on the top ($\sigma_2 = 36.79\,\mathrm{kg\,m^{-3}}$ for CM2G and $\sigma_2 = 36.63\,\mathrm{kg\,m^{-3}}$ for CM2M) that defines NADW. Transport out of the box is defined as positive. The balance is between the deep-water outflow at 49°N (denoted as "south") and inflow at Davis Strait and the GIS ridge (denoted as "north"). The residual is defined as transport through the isopycnal surface on the top (denoted as "diap"). The purple boxes denote the amount of transport contributed by the overflow and Labrador Sea diapycnal transport [integrated in the Labrador Sea box (in Fig. 3)] in "north" and "diap," respectively.

near-bottom stratification caused by different numerical mixing between the two models (e.g., Wang et al. 2015).

c. *Arctic freshwater export*

Comparing the two models, CM2G has a much larger freshwater export from the Arctic to the Atlantic via both outlets (Table 1). Although the CAA channels are much narrower in CM2G, the CM2G CAA freshwater transport is greater than CM2M.

The partitioning of freshwater transport between the CAA and Fram Strait is also different in the two models. In CM2G, freshwater transport through the CAA is more than 30% larger than that through Fram Strait, despite the latter's wider channel and stronger barotropic transport. In CM2M, CAA freshwater transport is only about 55% of Fram Strait transport.

Differences between CM2G and CM2M Labrador Sea convection, AMOC, and freshwater transports suggest potential differences in the model climates' responses to changes in freshwater routes, which will be examined through perturbation experiments described in the next section.

4. Experiment design

To test the hypothesis that the freshwater partition between the two major pathways via the CAA and Fram Strait impacts the Labrador Sea convection and AMOC, the topography near the channels in each model is modified to restrict the transport through each route. All experiments are listed in Table 2.

Referenced to the control simulations, three perturbation experiments are performed in CM2G. In the first experiment, CAA channels are closed (CLOSED_CAA_G) at their narrowest points in the model (Lancaster Sound, Cardigan Strait/Hell Gate, and Kennedy Channel; indicated by red lines in Fig. 2a) by setting the channel widths to zero.[4] In a second experiment (WIDE_CAA_G),

[4] With this change, only the channel width in the ocean model is modified and the grid in the ice model is kept the same so that ice transport is still allowed. See Adcroft (2013).

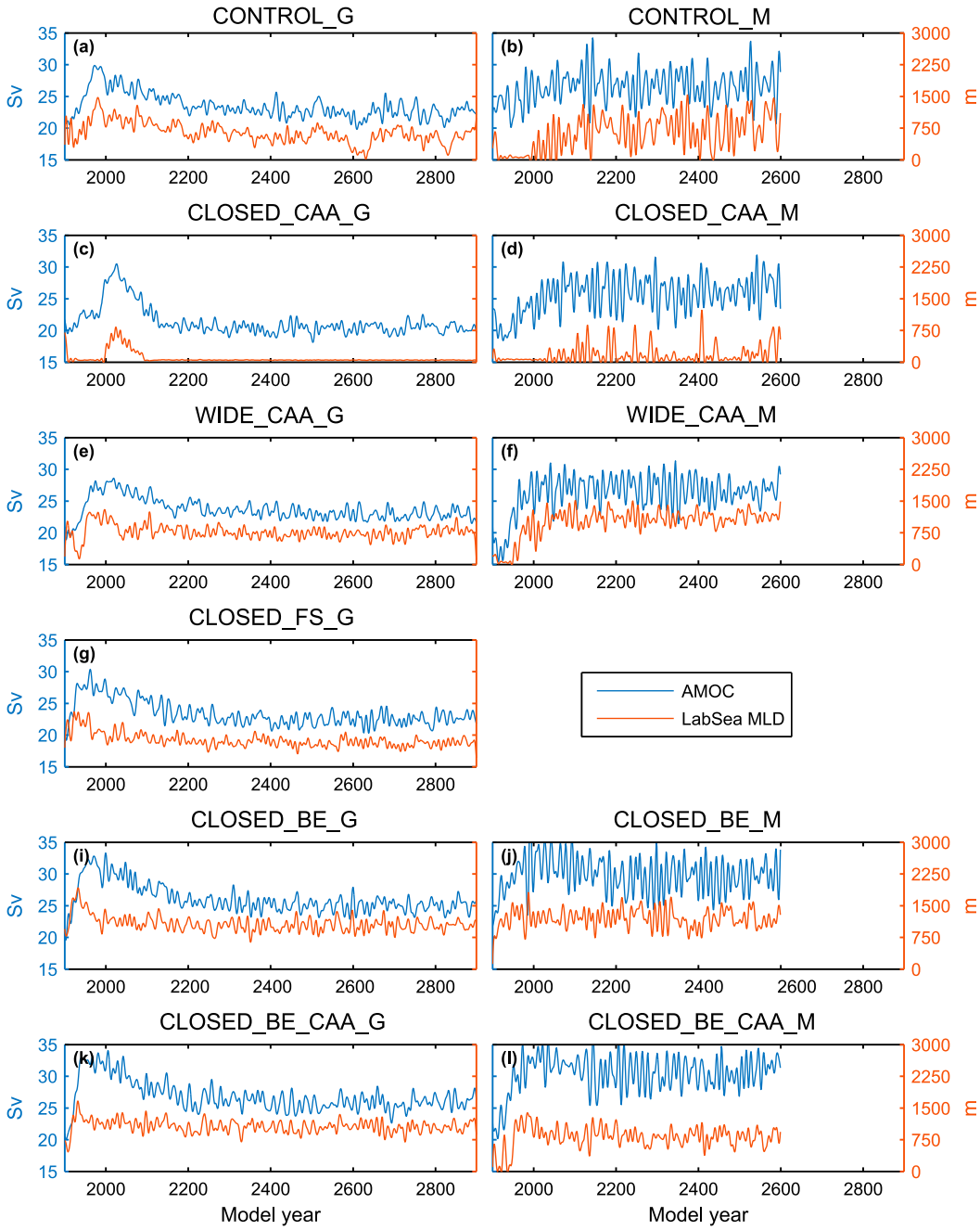

FIG. 5. AMOC index (blue) measured as the maximum streamfunction in density space at 49°N and area-averaged March MLD (orange) in the Labrador Sea, from both (left) CM2G and (right) CM2M. From top to bottom: (a),(b) control simulations, (c),(d) closed CAA experiments, (e),(f) widened CAA experiments, (g) closed FS experiment from CM2G, (i),(j) closed Bering Strait experiments, and (k),(l) closed both Bering Strait and CAA channels experiments. The streamfunctions are calculated with density (σ_2) as the vertical coordinate. The MLD is averaged over the domain of maximum convection in the Labrador Sea denoted in Fig. 3. For the purpose of a better presentation, an 11-point low-pass filter is applied to all time series to smooth out variability shorter than 10 years.

CAA transport is increased by creating a single wide and deep channel: an eight-grid cell (about 343 km)-wide and 300-m-deep channel near the region of Parry Channel, Jones Sound, and Devon Island (green box in Fig. 2a). Such extreme width and depth values for the artificial channel ensure a significant change in the freshwater transport, which is largely controlled by along-channel pressure gradient rather than channel

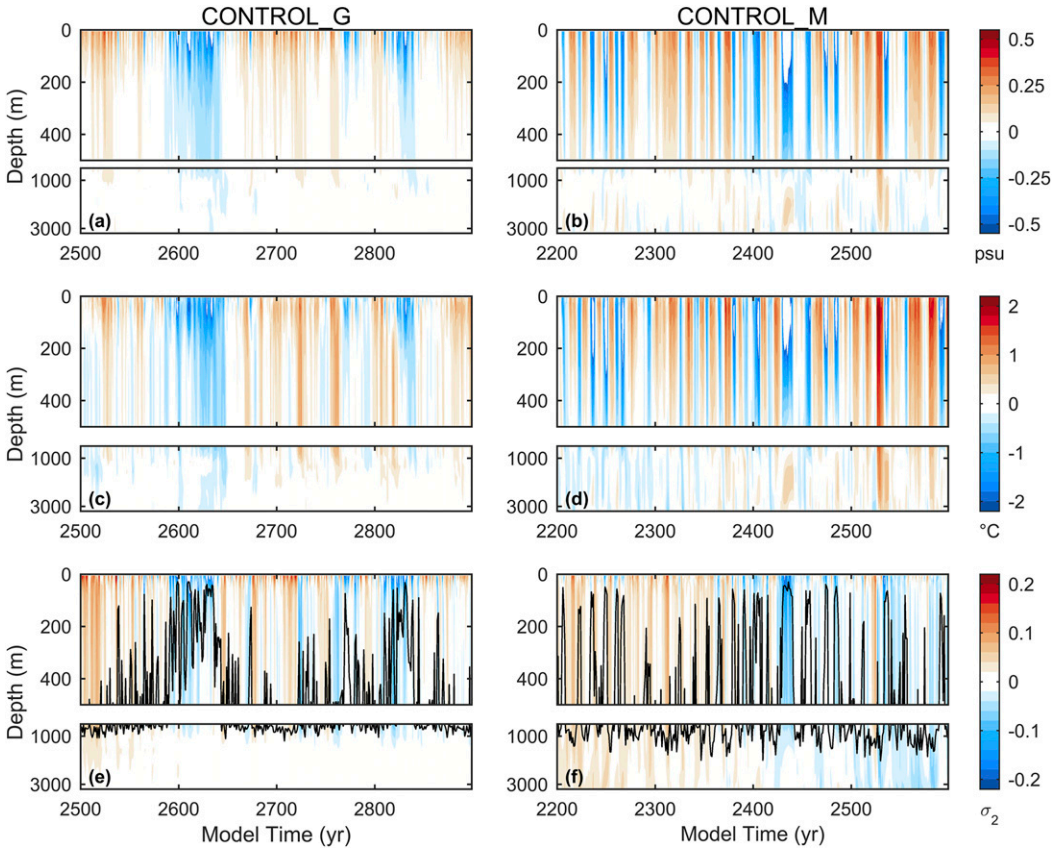

FIG. 6. Vertical profiles of time (annually) and area-averaged Labrador Sea (top row) salinity (psu), (middle row) temperature (°C), and (bottom) density (σ_2) anomaly as functions of time from (left) CONTROL_G and (right) CONTROL_M. The box region for averaging is shown in Fig. 3. For each model, only the last 400 years of simulation are shown. The black lines in (e) and (f) denote the depths of March MLD.

width. A third supplemental experiment (CLOSED_FS_G) is performed to reduce oceanic transport via Fram Strait, by lifting the topography to 10-m deep between Greenland and Svalbard (red box in Fig. 2a). Note that additional effects other than changes in surface freshwater transport are expected in this experiment, as dense water exchange between the Arctic and the Nordic seas via Fram Strait will also be reduced. Similarities between CLOSED_FS_G and WIDE_CAA_G will indicate the robustness of the impacts of increased western-route freshwater transport.

Similar changes of channel width are also implemented in CM2M to evaluate the sensitivity of the response to the mean-state climate and examine the robustness of the results. Experiments with closed/widened CAA channels (CLOSED_CAA_M and WIDE_CAA_M) are performed in CM2M in the same manner as in CM2G. In CLOSED_CAA_M, two adjacent ocean grid cells are replaced by land grid cells at Barrow Strait of Parry Channel and Smith Sound of Nares Strait. This modification also blocks ice transport, although the ice transport through the CAA is rather small in CM2M. In WIDE_CAA_M, a wide and deep channel with similar width and depth as in WIDE_CAA_G is implemented to allow more freshwater to flow through the CAA.

A further set of experiments are performed with a closed Bering Strait in both CM2G and CM2M. The Bering Strait acts as a freshwater source to the Arctic and the North Atlantic, and therefore plays an important role in the global climate (Hu et al. 2015). Closing Bering Strait reduces the total freshwater transport into the North Atlantic via both the CAA and Fram Strait. Performing similar experiments under the closed Bering Strait scenarios can potentially reduce the freshwater perturbation that is repartitioned between the two pathways.

Unless otherwise stated explicitly, we use the climatology of the last 200 years from both control and sensitivity experiments in the rest of the paper for comparison.

TABLE 2. List of experiments.

	Control	Closed CAA	Widened CAA	Closed Fram
Open Bering	CONTROL_G	CLOSED_CAA_G	WIDE_CAA_G	CLOSED_FS_G
	CONTROL_M	CLOSED_CAA_M	WIDE_CAA_M	
Closed Bering	CLOSED_BE_G	CLOSED_BE_CAA_G		
	CLOSED_BE_M	CLOSED_BE_CAA_M		

5. Results

a. CM2G: Closed CAA channels

Freshwater transports through the western and eastern routes to the North Atlantic are repartitioned after the closure of the CAA channels, as shown in Table 1. The reduced 1.11-Sv CAA depth-integrated transport is entirely compensated by a significant increase of transport via Fram Strait and some reduction of the eastward transport at the Barents Sea opening. Freshwater leaving the Arctic now flows mostly through the Fram Strait where the transport increases by more than 80%. Both volume and freshwater transport at the Bering Strait, as well as the freshwater (including surface flux and river runoff) from the Arctic, have very small changes, suggesting that the upstream sources of the freshwater are not sensitive to the CAA closure.

1) CHANGES IN THE AMOC AND NORTH ATLANTIC DIAPYCNAL TRANSPORT

In response to these freshwater pathway changes, Labrador Sea convection is significantly suppressed after an initial adjustment, and volume transport by the AMOC is weakened by around 2.1 Sv averaged over the last 200 years of simulation (Fig. 5c). Decomposition of the transport budget in the North Atlantic (Fig. 4) shows that the approximately 2.1-Sv decrease in deep transport at 49°N is mostly explained by the change in diapycnal transport in the Labrador Sea, which almost decreases to zero in CLOSED_CAA_G. Other components of the NADW, on the other hand, remain mostly unchanged.

Diapycnal transport is shown as a function of density in each convectively active region (Fig. 7). The most significant change in CLOSED_CAA_G (red lines) is in the Labrador Sea, where diapycnal transport ceases at all density classes, indicating halted convection. In the other regions, although the diapycnal transport change at the density level used in the budget calculation in Fig. 4 is small, noticeable changes are seen in other density classes: both the Nordic seas and North Atlantic (outside of the Labrador Sea) show a decrease of diapycnal transport in lower-density classes and increase in higher-density classes. Downward diapycnal transport therefore shifts to higher-density classes, a result of changes in vertical density structure and related deep convection and interior mixing elaborated below.

2) CHANGES IN MLD AND SURFACE PROPERTIES

The reduction of diapycnal transport in all density classes in the Labrador Sea and lower-density classes in other regions is associated with significant changes in deep convection. As shown in Fig. 8a, reduced convection spreads over the entire Labrador Sea, as well as other convectively active regions along the path of freshwater anomalies carried by the western boundary currents (EGC and WGC), including the western Nordic seas and the Irminger Sea. On the other hand, positive MLD anomalies are found farther away from the boundary regions, including the eastern Nordic seas and eastern North Atlantic south of the Greenland–Iceland–Scotland (GIS) ridge. The net modification of the area-integrated diapycnal transports in the Nordic seas and North Atlantic excluding the Labrador Sea is small (Fig. 4).

Reduced Labrador Sea convection and AMOC transport are caused by a series of positive feedbacks in the North Atlantic, associated with changes in sea surface salinity (SSS), SST, and ice boundaries (Figs. 8d,g). Increased freshwater follows the eastern route entering the Labrador Sea and recirculates around the basin, transported by both mean flow and eddies (parameterized in these models) into the basin interior, reducing SSS and increasing stratification. Labrador Sea convection is therefore inhibited, leading to the reduction of deep-water formation, which feeds the lower branch of the AMOC. The weakened AMOC transports less salt into the North Atlantic, including the Labrador Sea, which in turn results in further enhanced stratification in the Labrador Sea. As the northward heat flux by the AMOC decreases, surface temperature in the North Atlantic cools (Fig. 8g), encouraging ice formation. Oceanic convection is then further reduced by extended surface ice cover. As a result, the changes induced by weakened Labrador Sea convection are amplified by the AMOC-convection and ice-convection positive feedbacks, leading to the significant change of SST and SSS.

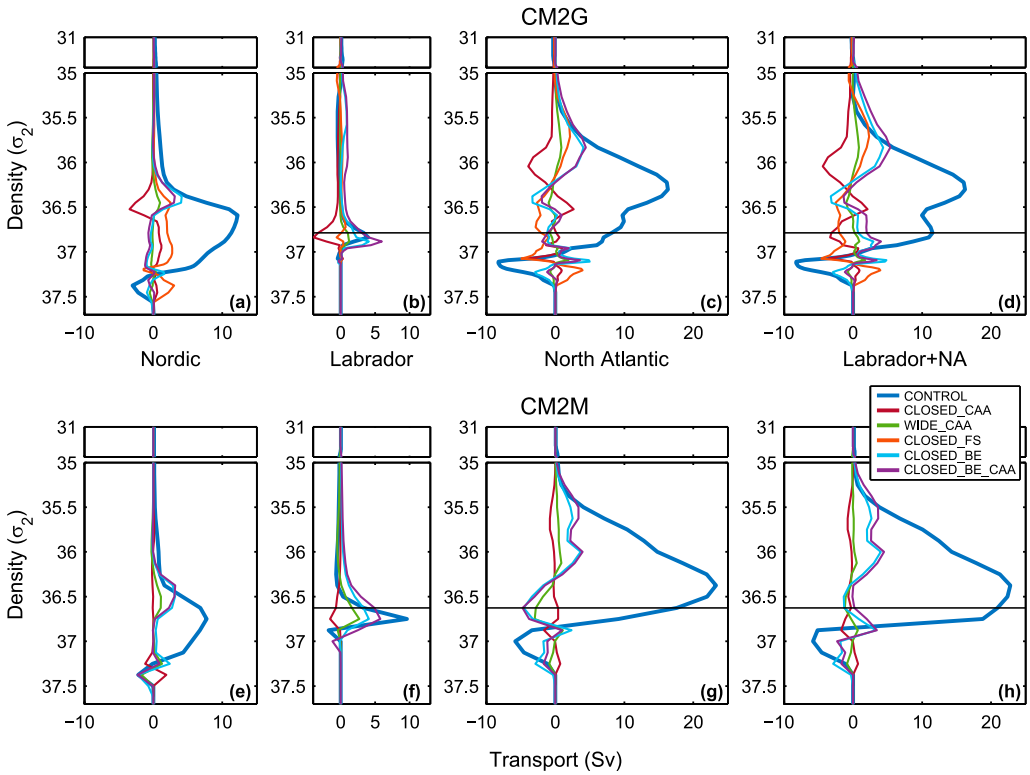

FIG. 7. Regionally integrated diapycnal transport as a function of density in (a),(e) the Nordic seas, (b),(f) the Labrador Sea, (c),(g) the North Atlantic south of the GIS ridge excluding the Labrador Sea, and (d),(h) all the North Atlantic south of the GIS ridge, for (top) CM2G and (bottom) CM2M. Results from CONTROL_G and CONTROL_M are shown in thick blue lines. Changes in perturbation experiments referenced to control simulations are shown in thinner lines (closed CAA channels in red, widened CAA channel in green, closed Fram Strait in orange, closed Bering Strait in cyan, and closed both Bering Strait and CAA channels in purple). Black lines indicate isopycnals used for budget calculation in Fig. 4. The boundaries of area integral are denoted as yellow lines in Fig. 3.

Within the Labrador Sea, the reductions of SSS and SST are not homogenous: the signal is much weaker along the western boundary. In fact, with less freshwater transport from the CAA along the western boundary, salinity is increased from the exit of the CAA channels to the western boundary of Baffin Bay. Unlike the decreased salinity in the eastern part of the Labrador Sea, the increased salinity in the west is confined along the boundary without much impact on the central Labrador Sea.

In the eastern part of the North Atlantic and the Nordic seas, MLD increases except in regions directly affected by the freshwater anomaly. Different regions show different sensitivity of the near-surface density to temperature and salinity, as shown in Fig. 9, affecting the sign of the MLD response.

The broadly cooler and fresher ocean surface caused by the reduced AMOC leads to negative and positive density anomalies in the Labrador Sea and rest of the North Atlantic, respectively. Further, density is reduced between 500- and 2000-m depth because of the trapped heat flux caused by suppressed convection. Therefore, in the eastern North Atlantic, the stratification in the interior ocean is weakened, encouraging mixing.

In the Nordic seas, a similar mechanism applies. Thus, with closed CAA channels, diapycnal mixing in both the Nordic seas and the North Atlantic (excluding the Labrador Sea) weakens in lower-density classes and strengthens in higher-density classes (Fig. 7). These changes outside of the Labrador Sea enhance deep-water formation and partially mitigate the direct effect of inactive convection in the Labrador Sea.

3) ATMOSPHERE–OCEAN COUPLING

The changes in North Atlantic convection are also assisted by coupling with the atmosphere. Reduced convection and increased ice cover reduce heat loss to the atmosphere in the Labrador Sea (Fig. 8j). On the other hand, in regions with enhanced convection (the eastern Nordic seas and the North Atlantic excluding the Labrador Sea), heat loss is increased, leading to a

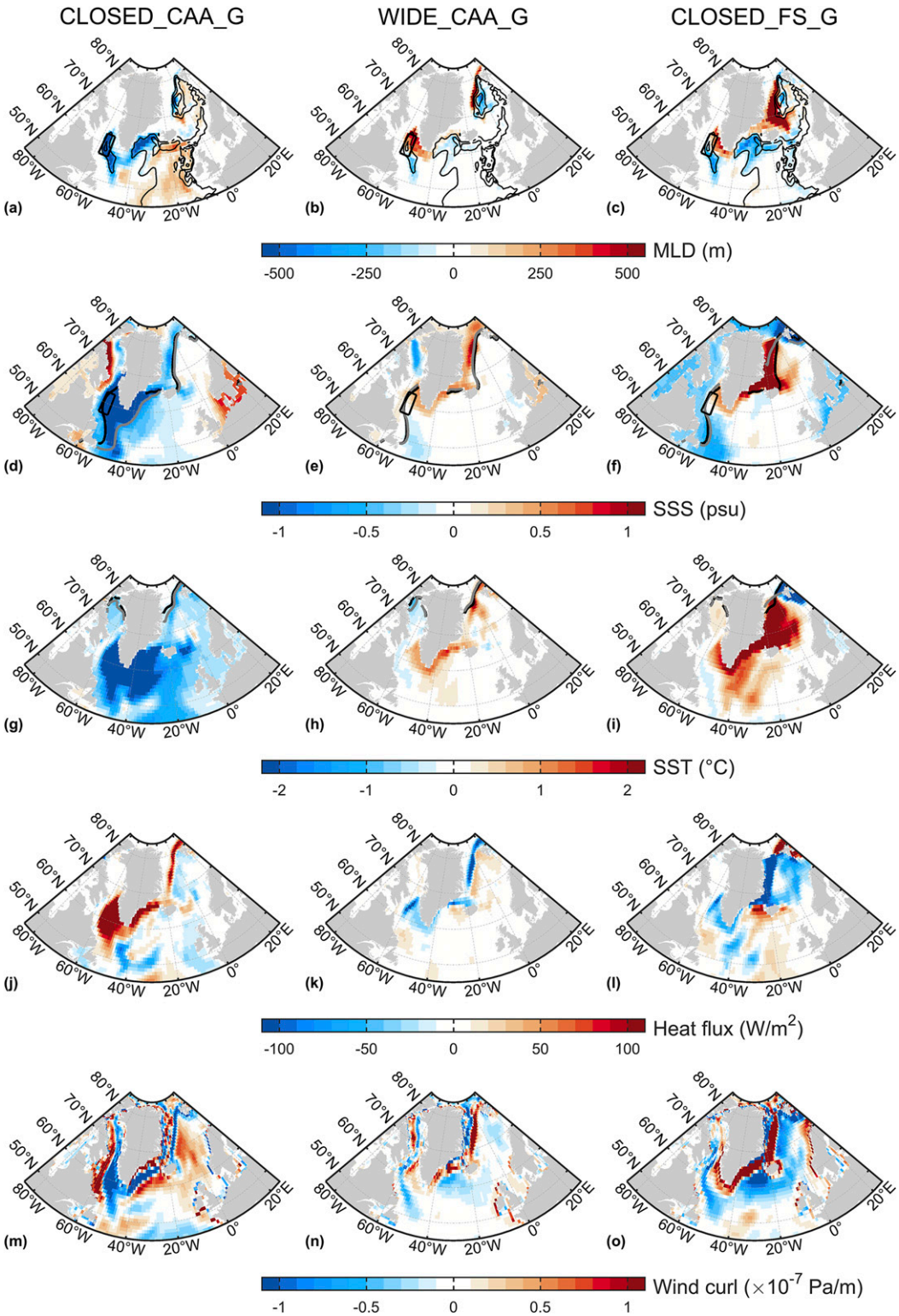

FIG. 8. Changes (perturbation − control) in (first row) March MLD (m), (second row) SSS (psu), (third row) SST (°C), (fourth row) wintertime (December–March) surface heat flux into the ocean (W m^{-2}; positive value means positive heat flux anomaly into the ocean), and (fifth row) surface wind stress curl (Pa m^{-1}) from (left) CM2G closed CAA experiment (CLOSED_CAA_G), (center) CM2G widened CAA experiment (WIDE_CAA_G), and (right) CM2G closed FS experiment (CLOSED_FS_G). Mean MLD from control simulation is superimposed as contoured lines on MLD anomaly with an interval of 200 m. March and September ice boundaries (15% of ice concentration) from control (black lines) and perturbation (gray lines) experiments are superimposed on SSS and SST anomalies, respectively.

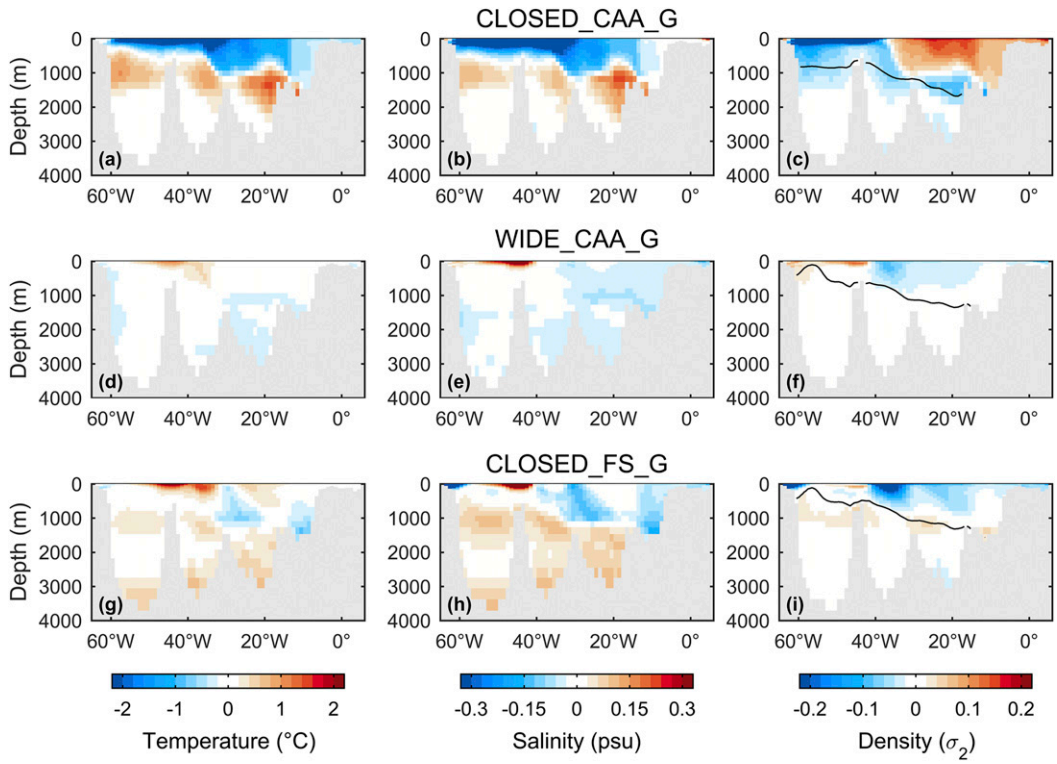

FIG. 9. Vertical profiles of changes (perturbation − control) in (left) temperature (°C), (center) salinity (psu), and (right) density (σ_2) from (top row) CM2G closed CAA experiment (CLOSED_CAA_G), (middle row) CM2G widened CAA experiment (WIDE_CAA_G), and (bottom row) CM2G closed FS experiment (CLOSED_FS_G). The location of density criterion used in Fig. 4 is denoted by the black lines in density plots. The profile is along the latitude of 59.5°N, which is across the North Atlantic including the center Labrador Sea.

smaller decrease in SST (Fig. 8g). Wind stress curl (Fig. 8m) is decreased in most of the Labrador Sea and other regions where convection and heat loss are reduced. By contrast, in the regions outside of the Labrador Sea, a positive wind stress curl anomaly is seen (Fig. 8m). Preconditioning for deep convection is thus favored through Ekman suction, proportional to the wind stress curl.

4) SUMMARY

In response to closed CAA channels, the strength of Labrador Sea convection is reduced and the AMOC is weakened; the effect of increased freshwater transport via the eastern route overcomes the effect of decreased freshwater transport via the western route. The model's Labrador Sea convection, strongest at the center of Labrador Sea, appears to be more sensitive to the positive freshwater anomaly via the eastern route.

At the same time, there is some compensation of deep-water formation, with increased convection outside of the regions directly influenced by the freshwater anomaly, because of a cooler climate and coupling with the atmosphere. The next section examines results from two experiments where freshwater transport is increased via the western route and decreased via the eastern route to further test the robustness of this sensitivity to freshwater pathways.

b. *CM2G: A widened CAA channel and closed Fram Strait*

Results of the previous section suggest that the effect of freshwater anomalies from the western route on Labrador Sea convection is limited compared with the eastern route. To further test this hypothesis, two simulations (WIDE_CAA_G and CLOSED_FS_G) are performed to allow more freshwater to flow through the CAA rather than via Fram Strait.

Depth-integrated volume and freshwater transport via the CAA increase in both WIDE_CAA_G and CLOSED_FS_G. The volume transport increase (Table 1) is larger in WIDE_CAA_G (1.08 Sv), compared with CLOSED_FS_G (0.87 Sv), while the freshwater transport increase in WIDE_CAA_G (37 mSv) is smaller than that of CLOSED_FS_G (72 mSv). As in CLOSED_CAA_G, the Bering Strait transport in WIDE_CAA_G hardly changes, while in CLOSED_FS_G it is reduced in both volume and freshwater inflow.

1) Changes in the AMOC and North Atlantic diapycnal transport

In both experiments, time-averaged AMOC transport is similar to that of the control simulation (averaged over the last 200 years, CONTROL_G is 22.5 Sv, WIDE_CAA_G is 22.9 Sv, and CLOSED_FS_G is 22.5 Sv; Figs. 5e,g). However, unlike the control run, there is no period of Labrador Sea convection shutdown, suggesting a more robust deep-water formation and AMOC. Despite unchanged AMOC strength, Labrador Sea MLD increases in WIDE_CAA_G, while that of CLOSED_FS_G is similar to CONTROL_G.

The unchanged AMOC transport is the result of a balance of changes in each component. In WIDE_CAA_G, diapycnal transport in the Labrador Sea significantly increases in all density classes, while that in the rest of the North Atlantic increases slightly in lower-density classes and decreases in higher-density classes (Fig. 7), leading to a net decrease (Fig. 4) in contrast to the changes in CLOSED_CAA_G.

CLOSED_FS_G has a rather different change in diapycnal transport. In the Nordic seas, the diapycnal transport increases because of additional warm and salty North Atlantic water trapped by the raised Fram Strait, which is balanced by a reduction in diapycnal transport south of the GIS ridge. CLOSED_FS_G shows similar changes outside of the Labrador Sea to those of WIDE_CAA_G, and similar diapycnal transport increase in lower-density classes within the Labrador Sea. However, the changes in Labrador Sea diapycnal transport are much smaller in CLOSED_FS_G and the maximum diapycnal transport is in fact slightly reduced, possibly associated with differences in freshwater changes and corresponding surface properties.

2) Changes in MLD and surface properties

MLD and surface property changes in CLOSED_FS_G and WIDE_CAA_G (right two columns in Fig. 8) are generally the opposite of the changes in CLOSED_CAA_G. Convection increases along the positive salinity (less freshwater) anomaly pathway from Fram Strait, resulting in increased MLD (Figs. 8b,c) along the Greenland coast and northwestern part of the Labrador Sea. In both experiments, positive SSS anomalies are seen along the Greenland coast and extending into the Labrador Sea (Figs. 8e,f). Along the western route, negative SSS anomalies are noticeable along the western boundary of Baffin Bay extending south into the Labrador Sea. The freshening signal stays close to the western boundary, away from the center of the convection region.

MLD is decreased on the western boundary of the Labrador Sea and Irminger Sea offshore of the Greenland coast in both experiments. Freshwater from the CAA carried along with the LC leaves the western boundary and enters the Labrador Sea farther downstream, resulting in the decrease of convection centered at 56°N, 51°W. The freshwater anomaly becomes diffuse but still visible leaving the Labrador Sea. Therefore, it is possible that the freshwater anomaly recirculates in the subpolar gyre, resulting in a decrease of convection in the Irminger Sea (Figs. 8b,c). The reduction of salinity is responsible for increased stratification in the eastern North Atlantic (Fig. 9). As the freshwater perturbation from the CAA is stronger in CLOSED_FS_G (Table 1), the anomalies in surface properties are also stronger, leading to a shallower averaged Labrador Sea MLD and convection compared with WIDE_CAA_G. In both CLOSED_FS_G and WIDE_CAA_G, the diapycnal transport outside of the Labrador Sea is reduced, with a stronger reduction in the former.

As in CLOSED_CAA_G but with the opposite sign, in WIDE_CAA_G and CLOSE_FS_G the atmosphere also helps to maintain the decreased MLD outside of the Labrador Sea. A negative surface wind stress curl anomaly, weakening convection, and reducing heat loss is seen in regions outside of the Labrador Sea and the Nordic seas (Figs. 8n,o).

A major difference between WIDE_CAA_G and CLOSED_FS_G is the large SSS/SST anomalies in the Nordic seas in CLOSED_FS_G. Closing Fram Strait blocks relatively warm and salty North Atlantic water from entering the Arctic. With the North Atlantic inflow trapped in and circulating around the Nordic seas, convection is greatly strengthened. Thus, even though in the Nordic seas the wind stress anomaly does not favor convection, enhanced heat loss associated with stronger convection is still found in CLOSED_FS_G (Fig. 8l). The strengthened deep-water formation in the Nordic seas therefore results in stronger overflow transport at Denmark Strait and Iceland–Scotland channels (Table 1 and Fig. 4).

3) Summary

CLOSED_FS_G and WIDE_CAA_G share similarities in changes of surface properties, including MLD, SSS, SST, and ice boundary, which are the opposite of the changes in CLOSED_CAA_G. Labrador Sea convection is enhanced in response to reduced freshwater from the eastern route. Strengthened convection results in a more robust AMOC. The effect of increased freshwater from the western route on open-ocean convection is limited and localized. These results support the hypothesis that freshwater via the eastern route has a

larger impact on the suppression of Labrador Sea convection.

At the same time, the AMOC does not exhibit a significant increase in either experiment. The increase of deep-water formation in the stronger convection region is largely compensated by a decrease of diapycnal transport in the rest of the North Atlantic. The compensation of convection changes outside of the region directly influenced by the freshwater anomaly is similar to previous results from localized water-hosing experiments (e.g., Saenko et al. 2007). The change of Irminger Sea convection due to the repartition of freshwater forcing is not symmetric between the freshwater routes: it is reduced in all three experiments. Located near the path of the eastern route, additional freshwater export via Fram Strait impacts the Irminger Sea convection first before Labrador Sea. Freshwater forcing from the CAA does not affect the Labrador Sea, but may reduce the surface density in the Irminger Sea via transport around the subpolar gyre.

c. CM2M

In the previous section, we showed that in CM2G freshwater transported via the eastern route more effectively suppresses Labrador Sea convection. To further test the robustness of the results and evaluate the model dependence of the AMOC response, two similar experiments (CLOSED_CAA_M and WIDE_CAA_M) are performed in CM2M.

The depth-integrated and freshwater transport via the CAA decreases and increases in CLOSED_CAA_M and WIDE_CAA_M, respectively. In CLOSED_CAA_M, most of the CAA transport is diverted to Fram Strait. In WIDE_CAA_M with a widened and deepened channel, CAA freshwater transport doubles (smaller than the WIDE_CAA_G increase, despite the total transport increase of almost 2 Sv, roughly twice the increase in WIDE_CAA_G). As in the CM2G experiments, Bering Strait and other freshwater sources in the Arctic remain unchanged in both CM2M experiments.

Changes in deep-water formation, associated surface properties, and air–sea interaction in CM2M experiments are very similar to those in CM2G (Figs. 10 and 11), which results in the opposite changes to convection within the Labrador Sea and outside of it (Fig. 4).

In contrast to the CM2G experiment, however, the strength of the AMOC in both CLOSED_CAA_M and WIDE_CAA_M remains almost unchanged compared with CONTROL_M, despite the repartition of freshwater via the eastern and western routes. The small change of AMOC transport is the result of the compensating effect of convection changes in the North Atlantic. In both CM2M experiments, changes in Labrador Sea convection are mostly compensated by changes in other regions (Fig. 4), resulting in a small net change in the total North Atlantic diapycnal transport (Fig. 7g).

This difference in the AMOC response between CM2M- and CM2G-based experiments suggests that in CONTROL_M, although surface properties and various components of the NADW are subjected to similar changes compared with CONTROL_G, the AMOC is more resistant to the repartition of freshwater transport via the western and eastern routes. The positive feedbacks in the Labrador Sea that would trigger a significant reduction of the AMOC are overcome by the compensation effect of convection in the rest of the North Atlantic. Various factors may contribute to this difference of the AMOC response between the two models, including the differences in the mean-state Labrador Sea convection and freshwater forcing induced by closing or widening the channel. In the following section, a different North Atlantic climate is introduced in both models by closing the Bering Strait to further test the sensitivity of the response of the AMOC as a function of mean-state climate.

d. A closed Bering Strait scenario

The differences between the CM2G- and CM2M-based experiment results suggest that the response of North Atlantic convection and the AMOC to changes in the Arctic freshwater pathway is sensitive to the differences in mean-state climate, specifically the amount of freshwater transport through the CAA and MLD. These conditions can be modified by closing the Bering Strait. Previous research (De Boer and Nof 2004; Hu et al. 2012, 2015; Otto-Bliesner et al. 2017) suggests that opening the Bering Strait impacts the strength and stability of the AMOC; Hu et al. (2015) found that the AMOC is significantly strengthened with a closed Bering Strait because of reduced freshwater import leading to enhanced North Atlantic convection. In this section, we first evaluate the changes in mean-state climate with a closed Bering Strait, then repeat the closed CAA experiment in both CM2G and CM2M under the new climatology.

1) CLIMATOLOGY

With a closed Bering Strait, the AMOC magnitude is enhanced significantly in both models (at 49°N, the increase in transport is 2.4 Sv for CM2G and 2.9 Sv for CM2M; Figs. 5i,j) because of increased overflow transport and diapycnal transport in the Labrador Sea (Fig. 4). These changes are partially compensated by decreases in diapycnal transport outside of the Labrador Sea.

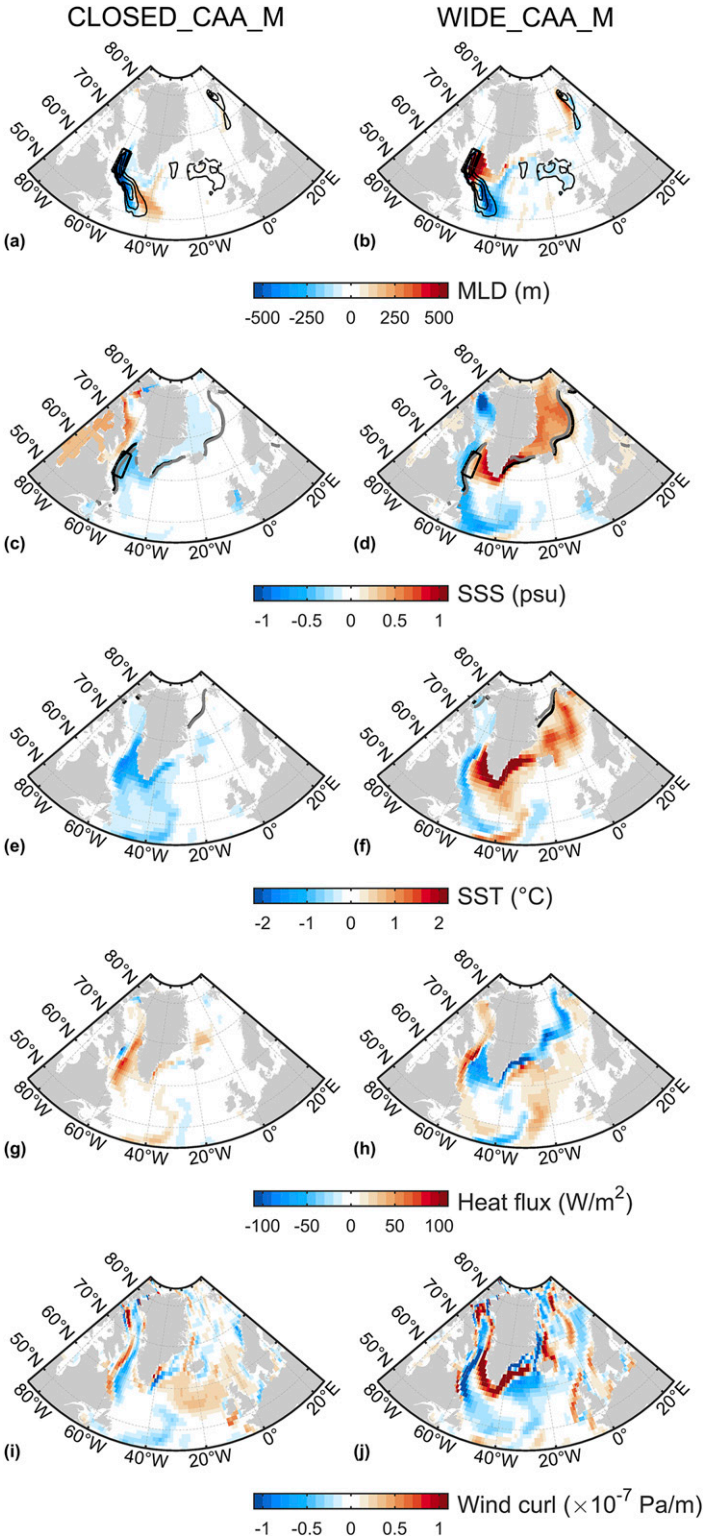

FIG. 10. As in Fig. 8, but for experiments (closed and widened CAA) based on CM2M.

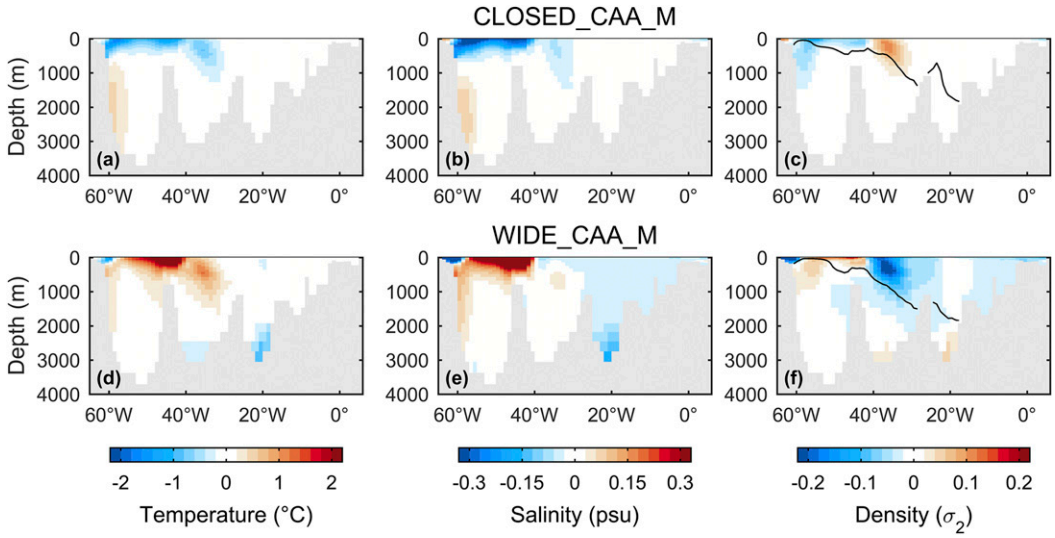

FIG. 11. As in Fig. 9, but for experiments based on CM2M.

With a stronger AMOC, the North Atlantic sea surface warms and the ice boundary retreats (Fig. 12). Without the Bering Strait source of freshwater, SSS in the Arctic and North Atlantic increases significantly, consistent with Hu et al. (2015). Comparing the two models with closed Bering Strait, the SST anomaly in CLOSED_BE_M is generally larger than in CLOSED_BE_G because of a stronger AMOC, which leads to enhanced northward heat transport. The SSS anomaly is larger in CLOSED_BE_G because of the larger freshwater change induced by the Bering Strait closure (Table 1).

The relative changes of outflowing Arctic freshwater also vary in the eastern and western route, reflected in

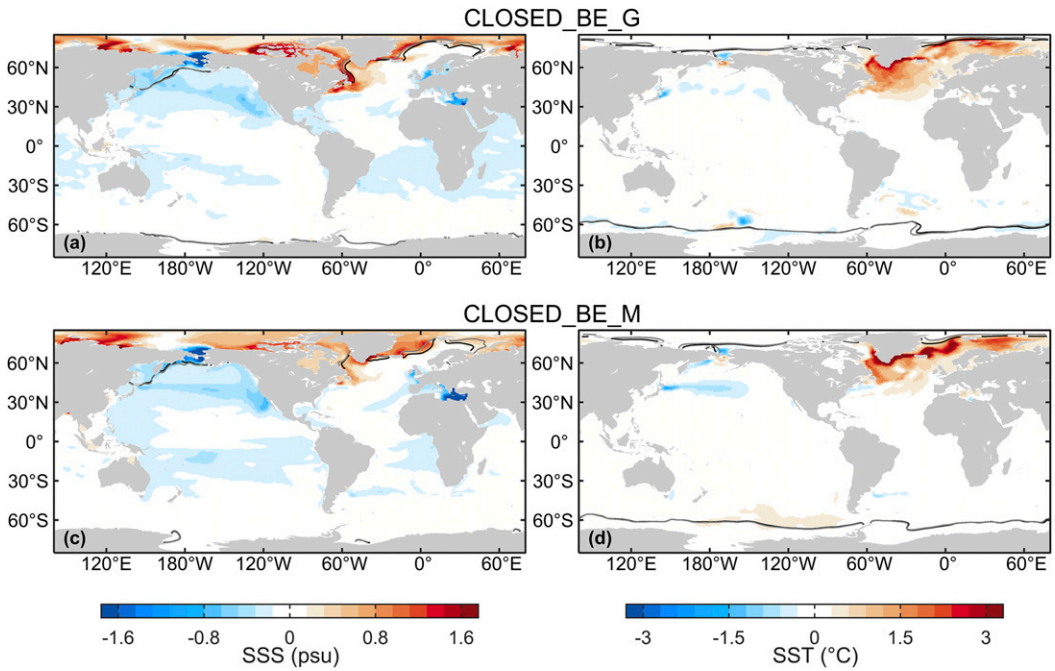

FIG. 12. Changes in (left) SSS (psu) and (right) SST (°C) in (upper panel) CLOSED_BE_G and (lower panel) CLOSED_BE_M relative to control runs. March and September ice boundaries (15% ice concentration) from closed Bering Strait (gray) and control (black) are also shown on SSS and SST maps, respectively.

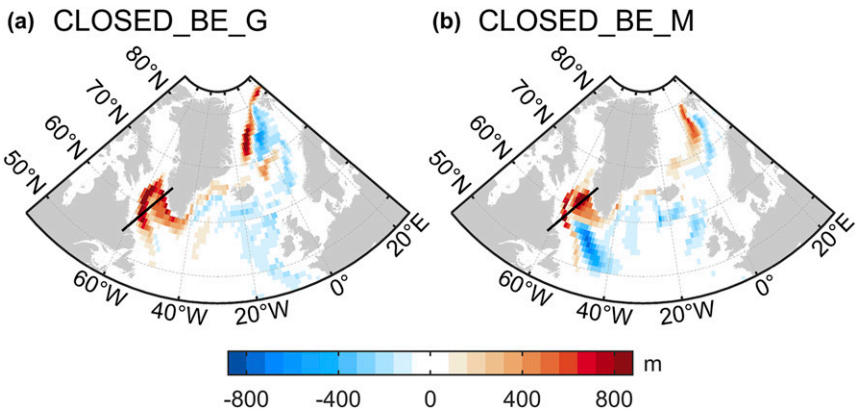

FIG. 13. Changes in MLD from closed Bering Strait experiments in (left) CLOSED_BE_G and (right) CLOSED_BE_M relative to control. The black lines denote the locations of the vertical profile shown in Fig. 15.

the SSS anomaly spatial distribution. In both models, Fram Strait has a larger reduction in liquid and ice freshwater transport than the CAA. Comparing the two models, CAA freshwater reduction is much larger in CLOSED_BE_G than in CLOSED_BE_M. Thus, the positive SSS anomaly signal along the western boundary of the Labrador Sea is larger in CLOSED_BE_G than in CLOSED_BE_M.

With a comparatively stronger decrease of freshwater transport via the eastern route, the horizontal distribution of the changes in MLD (Fig. 13) resembles that in the widened CAA channel experiments (Figs. 8b and 10b). At the same time, in the closed Bering Strait experiments, enhanced convection is also observed along the western boundary of the Labrador Sea because of the simultaneous reduction in freshwater export through the CAA.

2) Closed CAA channels with closed Bering Strait

We perform closed CAA experiments (CLOSED_BE_CAA_G and CLOSED_BE_CAA_M) under this new climate with a weaker Arctic freshwater export and a stronger AMOC. Since Bering Strait transport is not affected by the changes in the CAA (Table 1), we assume the difference between the climatic response in CLOSED_CAA_G(M) and CLOSED_BE_CAA_G(M) is mostly due to the changes in mean-state climate, rather than further coupling between a closed Bering Strait and the CAA.

In CLOSED_BE_CAA_G and CLOSED_BE_CAA_M, the relative changes in freshwater transport through the CAA and Fram Strait are different from their open Bering Strait counterparts. In CLOSED_BE_CAA_G, the 28-mSv increase in Fram Strait freshwater export, relative to CLOSED_BE_G, is much smaller than the increase in CLOSED_CAA_G (65 mSv). In CLOSED_BE_CAA_M, the change in Fram Strait transport (22 mSv) is almost the same as in CLOSED_CAA_M (21 mSv).

The response of MLD and SSS (Figs. 14a–d) to the freshwater pathway changes from CLOSED_BE_CAA_G and CLOSED_BE_CAA_M are similar to the open Bering Strait experiments (top rows of Figs. 8 and 10): following SSS changes, MLD is reduced along the eastern route and interior Labrador Sea, and increased along the western route. Compared with the open Bering Strait cases, increased SSS and MLD from the western route are stronger in the western part of the Labrador Sea and farther downstream. For CLOSED_BE_CAA_G, no Labrador Sea convection collapse occurs in contrast to the open Bering Strait experiment, possibly because of a more robust Labrador Sea convection and AMOC in CLOSED_BE_G.

On the other hand, the AMOC in CLOSED_BE_CAA_G(M) increases compared with CLOSED_BE_G(M) (0.97 Sv for CLOSED_BE_CAA_G and 1.05 Sv for CLOSED_BE_CAA_M; Figs. 5k,l), in contrast with their open Bering Strait climate counterparts. The increased AMOC transport is mostly contributed by an enhanced diapycnal transport in the Labrador Sea (Fig. 4).

The seeming inconsistency between the changes in convection (measured by MLD) and diapycnal transport reflects the changes in relative importance of the location of deep-water formation. With a closed Bering Strait, near-surface density change is greater along the western boundary than the eastern boundary of the Labrador Sea (Figs. 15a,c). Therefore, the center of the Labrador Sea convection (maximum MLD) moves

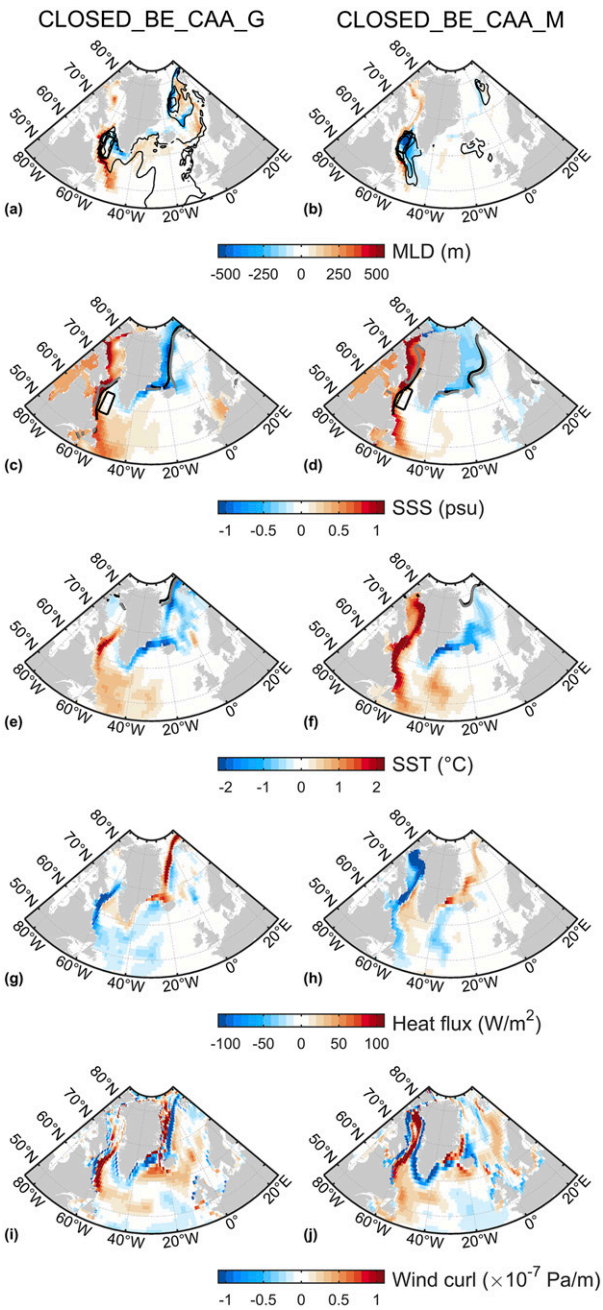

FIG. 14. As in Fig. 8, but for experiments CLOSED_BE_CAA_G and CLOSED_BE_CAA_M referenced to CLOSED_BE_G and CLOSED_BE_M.

closer to the western boundary, which makes it more sensitive to the freshwater forcing anomaly through the CAA.

Similar to open Bering Strait scenarios, closing CAA channels leads to shallower MLD in the eastern and central Labrador Sea and deeper MLD near the western boundary of the Labrador Sea (Figs. 15b,d and 14a,b). The net effect is that deep-water formation and downward diapycnal transport is increased in the Labrador Sea (Figs. 7b,f). This suggests that with a westward shift of the deep convection location in the Labrador Sea under the closed Bering Strait scenarios, the deep-water formation changes in the western Labrador Sea dominate over those in the central and eastern Labrador Sea.

For the North Atlantic outside of the Labrador Sea, SSS and SST increases (Figs. 14c–f) with a stronger AMOC. A relatively small increase of surface density occurs, and diapycnal transport in lower-density classes increases (Fig. 7).

Changes in the atmosphere largely agree with their open Bering Strait counterparts, except for the Labrador Sea and along the coast of Greenland (Fig. 14). While heat flux is reduced in the Labrador Sea, as in CLOSED_CAA_G and CLOSED_CAA_M, positive wind stress curl along the western boundary dominates the entire Labrador Sea in both experiments here. Outside of the Labrador Sea, wind stress curl anomalies that favor an enhanced convection are observed, similar to CLOSED_CAA_G and CLOSED_CAA_M.

3) SUMMARY

These perturbation experiments with a closed Bering Strait test the response to changes in freshwater pathways under a different climate. Changes in surface properties are generally consistent with their open Bering Strait counterparts. The responses of Labrador Sea diapycnal transport and the AMOC to these changes at the surface, however, are different; sensitivity of Labrador Sea convection is now dominated by the western boundary. In response, diapycnal transport increases in the Labrador Sea. At the same time, with similar compensation in deep-water formation outside of the Labrador Sea as in CLOSED_CAA_G and CLOSED_CAA_M, the AMOC transport becomes stronger, leading to a warmer climate and increased North Atlantic convection. These results, together with the differences between CLOSED_CAA_G and CLOSED_CAA_M, indicate the dependence of the AMOC's response to freshwater pathway change on the mean-state climate.

6. Discussion and conclusions

The relative influence of the freshwater export from the Arctic via two different pathways on Labrador Sea convection and the AMOC is studied using two coupled climate models. Freshwater from the Arctic can either follow the eastern route via Fram Strait, circumnavigating Greenland and entering the Labrador Sea at Cape Farewell, or the western route through the CAA

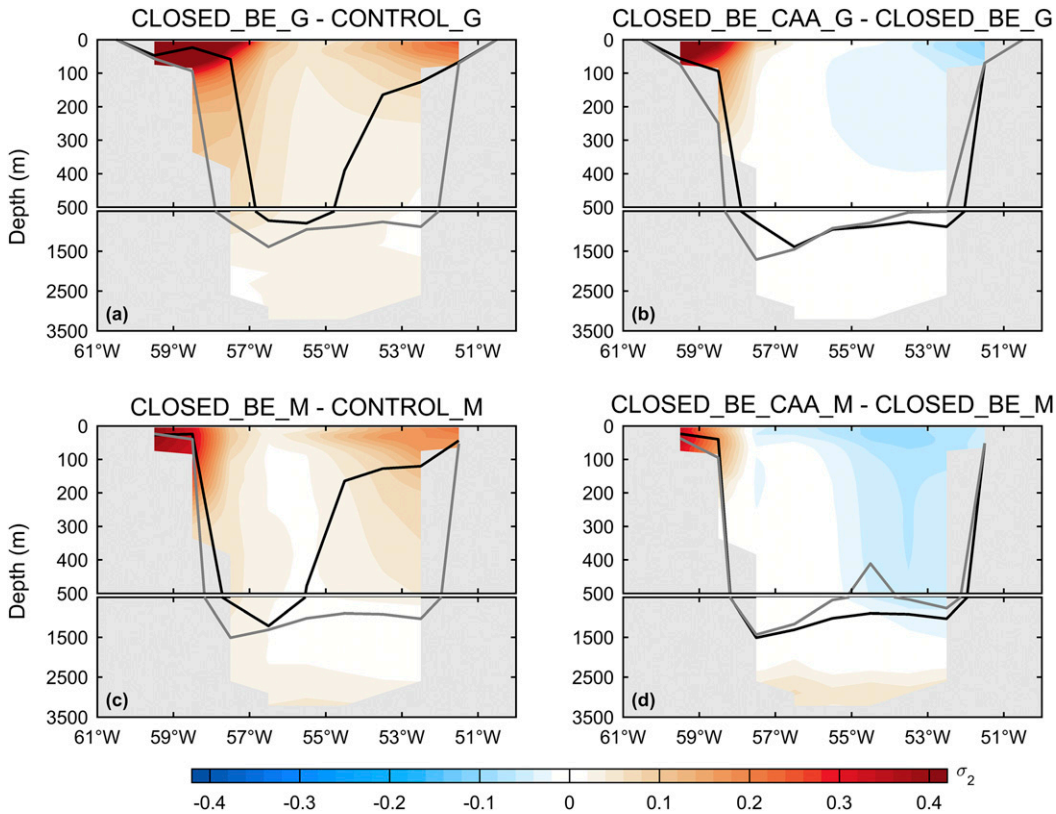

FIG. 15. Vertical profiles of changes in density (σ_2) across the Labrador Sea. (a),(c) Changes in closed Bering Strait experiments referenced to controls, and (b),(d) changes in closed CAA experiments with Bering Strait closed referenced in closed Bering Strait experiments. Positions of March MLD are denoted as black lines for controls [CONTROL_G and CONTROL_M for (a),(c) and CLOSED_BE_G and CLOSED_BE_M for (b),(d)], and gray lines for perturbations [CLOSED_BE_G and CLOSED_BE_M for (a),(c) and CLOSED_BE_CAA_G and CLOSED_BE_CAA_M for (b),(d)]. Location of the cross section is shown in Fig. 13.

and entering the Labrador Sea in the north directly upstream of the western boundary current. Results from two globally coupled models show that despite being a geographically more direct pathway into the Labrador Sea, freshwater flowing via the western route stays close to the western boundary and only interacts indirectly with Labrador Sea convection. Freshwater via the eastern route, which flows around a larger part of the Labrador Sea basin, has more interaction with the central Labrador Sea and suppresses convection. The conclusion is consistent with previous ocean-only modeling studies (e.g., Komuro and Hasumi 2005) and coupled modeling studies with paleoclimate boundary conditions (Otto-Bliesner et al. 2017).

In the control simulations, volume and freshwater transport through the CAA channels are different in CM2G and CM2M. The model CAA channels are wider in CM2M than in CM2G, but the volume and freshwater transports are smaller in CM2M. Rather than the specific model topography configuration and channel width, we find that the difference between the two models in CAA transport and partition between the CAA and Fram Strait depend on the model's mean climatology (including both oceanic and atmospheric general circulations in the Arctic region, not shown).

The present results are based on 1° climate models, which usually have difficulties in representing boundary currents. Boundary currents in coarse-resolution models are wider and slower than the real ocean. Thus, in finer-resolution models with narrower boundary currents, the effect of freshwater along the western boundary may be limited further. On the other hand, 1° climate models do not directly resolve mesoscale eddies, which are crucial for the exchange between boundary currents and the central Labrador Sea (although parameterizations of eddies are applied). Observations and high-resolution modeling studies do suggest active interaction between the WGC and the open ocean, while the interaction between the LC and open ocean is considered to be weaker (Eden and Böning 2002; Schmidt and Send 2007)

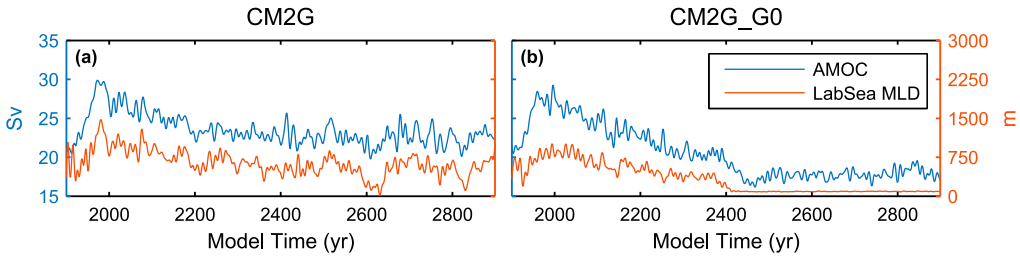

FIG. 16. As in Fig. 5, but for a comparison between CM2G control used here and a low-diffusivity CM2G simulation.

and located near the exit of the Labrador Sea (McGeehan and Maslowski 2011). In addition, simulations from CM2.5 and CM2.6, which are the higher-resolution versions of CM2M, suggest higher eddy kinetic energy near the eastern boundary of the Labrador Sea than the western boundary (Fig. 14 in Delworth et al. 2012).

Changes in Labrador Sea convection induced by changes of freshwater pathways do not necessarily impact the strength of the AMOC. In our experiments with different models and scenarios, a decrease or increase of Labrador Sea convection is accompanied by opposite changes outside of the Labrador Sea, which usually result in small net change of the NADW and AMOC transport. By using coupled models, we find that the opposite changes of the convection inside and outside of the Labrador Sea are assisted by corresponding changes of surface heat and momentum fluxes, which are processes not included in previous ocean-only models.

Comparing the results from CM2G and CM2M experiments, we find that the changes of the AMOC are sensitive to the mean-state climate. CM2M has relatively stronger convection in the Labrador Sea, which suggests that it is less susceptible to surface buoyancy change. Thus, the series of positive feedbacks that result in a drastic change of the AMOC in CM2G do not lead to similar changes in CM2M. In addition, the amount of freshwater anomaly induced by repartitioning the freshwater is smaller in CM2M, which further limits the Labrador Sea's response to freshwater forcing.

Here, we show further support that the sensitivity of the Labrador Sea to freshwater forcing may depend on the strength of the mean-state MLD. In a version of CM2G with a smaller, lower bound for diapycnal diffusivity, Labrador Sea convection shuts off after 500 years, leading to a significant reduction of the AMOC (Fig. 16). Compared with CONTROL_G, MLD in this low-diffusivity case is smaller. This suggests that a change in mean-state MLD could result in a change of sensitivity of the Labrador Sea convection.

Differences in mean-state Labrador Sea MLD could result from models' differing deep stratification. Figure 3 shows the distinction between the two models in the variability of Labrador Sea convection depth, where that in CM2M can reach a greater depth than in CM2G. This could be caused by the two models' differences in the Nordic seas overflows, which stem from their difference in vertical coordinates (Wang et al. 2015).

Changes in the subpolar gyre observed in CM2M-based experiments act to compensate changes in the Labrador Sea. With closed CAA channels and weakened Labrador Sea convection, the subpolar gyre is expanded and strengthened in CLOSED_CAA_M (Fig. 17a), which enhances the poleward heat flux and prevents the potential positive feedbacks that would lead to a complete shutdown of Labrador Sea convection and significant reduction of the AMOC, as in CLOSED_CAA_G. Similarly, a weakened subpolar gyre is observed with a widened CAA channel (Fig. 17b). Similar changes are not observed in the CM2G-based experiments. The different response of the subpolar gyre to freshwater forcing in the Labrador Sea may be relevant to differences in North Atlantic decadal variability between the two models, which involve the interaction between the AMOC and subpolar gyre transport (Delworth et al. 1993).

Further, the sensitivity of Labrador Sea convection to the partition of freshwater forcing also depends on the status of Bering Strait. In the scenarios with a closed Bering Strait, in which the climatological MLD is enhanced and total freshwater forcing is reduced in both models, the AMOC becomes stronger when freshwater forcing via Fram Strait is increased. Our results here agree with a recent study by Otto-Bliesner et al. (2017) with experiments under Pliocene boundary conditions: a closed CAA leads to a weakened AMOC when the Bering Strait is open, but when the Bering Strait is closed, closing the CAA leads to a strengthened AMOC. From the decomposition of different deep-water sources (Fig. 4), we find that the difference is largely attributed to the different response of deep water formed in the Labrador Sea. In a warmer North Atlantic and less total freshwater export from the Arctic,

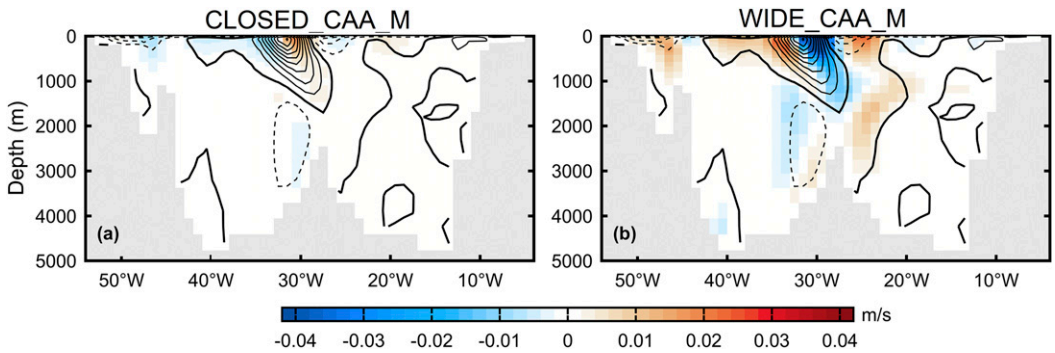

FIG. 17. Meridional velocity at 48.5°N from control simulation (contour lines, with an interval of 0.02 m s^{-1}) and changes in perturbation experiments (shaded colors) in (left) CLOSED_CAA_M and (right) WIDE_CAA_M.

diapycnal transport of deep water in the Labrador Sea increases with the closed CAA.

Irminger Sea deep convection in CM2G is as strong as that in the Labrador Sea, while it is much weaker in CM2M (Fig. 3). This difference may help explain the two models' different AMOC responses to additional freshwater from the eastern route, which passes through the Irminger Sea. The location of the Irminger Sea indicates that it is more susceptible to freshwater from the eastern route, which would downplay the effect of compensated convection change outside of the Labrador Sea. Deep water is observed in the Irminger Sea from both remote and local formation, although the local contribution is more sporadic (Våge et al. 2011). Model results here indicate that in the real ocean, the eastern-route freshwater anomalies during Irminger Sea convection events may at least cause a transient response of the AMOC.

In the real ocean, the freshwater anomaly caused by the melting of the Arctic sea ice and the Greenland ice sheet could effectively follow either the eastern or western route, depending on the discharge locations (Liu et al. 2018; Gillard et al. 2016; Dukhovskoy et al. 2016). Results here suggest that the sensitivity of the Labrador Sea convection to the two pathways is different. More importantly, indirect response to the freshwater anomaly could be triggered in other convectively active regions, where deep-water formation can be larger than the Labrador Sea (e.g., Pickart and Spall 2007). The direct and indirect response to the freshwater anomaly in the North Atlantic may be equally important to the changes in the AMOC.

Acknowledgments. We thank three anonymous reviewers for their comments that helped to improve the manuscript. We are also grateful to Drs. Stephen Griffies and Xiaoqin Yan for their useful comments on an earlier version of the paper. This paper was prepared under Award NA14OAR4320106 from the National Oceanic and Atmospheric Administration, U.S. Department of Commerce. The statements, findings, conclusions, and recommendations are those of the author(s) and do not necessarily reflect the views of the National Oceanic and Atmospheric Administration or the U.S. Department of Commerce.

REFERENCES

Aagaard, K., and E. C. Carmack, 1989: The role of sea ice and other fresh water in the Arctic circulation. *J. Geophys. Res.*, **94**, 14 485–14 498, https://doi.org/10.1029/JC094iC10p14485.

Adcroft, A., 2013: Representation of topography by porous barriers and objective interpolation of topographic data. *Ocean Modell.*, **67**, 13–27, https://doi.org/10.1016/j.ocemod.2013.03.002.

Belkin, I. M., 2004: Propagation of the "Great Salinity Anomaly" of the 1990s around the northern North Atlantic. *Geophys. Res. Lett.*, **31**, L08306, https://doi.org/10.1029/2003GL019334.

——, S. Levitus, J. Antonov, and S.-A. Malmberg, 1998: "Great Salinity Anomalies" in the North Atlantic. *Prog. Oceanogr.*, **41**, 1–68, https://doi.org/10.1016/S0079-6611(98)00015-9.

De Boer, A. M., and D. Nof, 2004: The exhaust valve of the North Atlantic. *J. Climate*, **17**, 417–422, https://doi.org/10.1175/1520-0442(2004)017<0417:TEVOTN>2.0.CO;2.

de Boyer Montégut, C., G. Madec, A. S. Fischer, A. Lazar, and D. Iudicone, 2004: Mixed layer depth over the global ocean: An examination of profile data and a profile-based climatology. *J. Geophys. Res.*, **109**, C12003, https://doi.org/10.1029/2004JC002378.

Delworth, T. L., S. Manabe, and R. J. Stouffer, 1993: Interdecadal variations of the thermohaline circulation in a coupled ocean–atmosphere model. *J. Climate*, **6**, 1993–2011, https://doi.org/10.1175/1520-0442(1993)006<1993:IVOTTC>2.0.CO;2.

——, and Coauthors, 2006: GFDL's CM2 global coupled climate models. Part I: Formulation and simulation characteristics. *J. Climate*, **19**, 643–674, https://doi.org/10.1175/JCLI3629.1.

——, and Coauthors, 2012: Simulated climate and climate change in the GFDL CM2.5 high-resolution coupled climate model. *J. Climate*, **25**, 2755–2781, https://doi.org/10.1175/JCLI-D-11-00316.1.

Dickson, R. R., J. Meincke, S.-A. Malmberg, and A. J. Lee, 1988: The "Great Salinity Anomaly" in the northern North Atlantic 1968–1982. *Prog. Oceanogr.*, **20**, 103–151, https://doi.org/10.1016/0079-6611(88)90049-3.

——, B. Rudels, S. Dye, M. Karcher, J. Meincke, and I. Yashayaev, 2007: Current estimates of freshwater flux through Arctic and subarctic seas. *Prog. Oceanogr.*, **73**, 210–230, https://doi.org/10.1016/j.pocean.2006.12.003.

Dukhovskoy, D. S., and Coauthors, 2016: Greenland freshwater pathways in the sub-Arctic seas from model experiments with passive tracers. *J. Geophys. Res. Oceans*, **121**, 877–907, https://doi.org/10.1002/2015JC011290.

Dunne, J. P., and Coauthors, 2012: GFDL's ESM2 global coupled climate–carbon Earth system models. Part I: Physical formulation and baseline simulation characteristics. *J. Climate*, **25**, 6646–6665, https://doi.org/10.1175/JCLI-D-11-00560.1.

Eden, C., and C. Böning, 2002: Sources of eddy kinetic energy in the Labrador Sea. *J. Phys. Oceanogr.*, **32**, 3346–3363, https://doi.org/10.1175/1520-0485(2002)032<3346:SOEKEI>2.0.CO;2.

Ganachaud, A., and C. Wunsch, 2000: Improved estimates of global ocean circulation, heat transport and mixing from hydrographic data. *Nature*, **408**, 453–457, https://doi.org/10.1038/35044048.

Gillard, L. C., X. Hu, P. G. Myers, and J. L. Bamber, 2016: Meltwater pathways from marine terminating glaciers of the Greenland ice sheet. *Geophys. Res. Lett.*, **43**, 10 873–10 882, https://doi.org/10.1002/2016GL070969.

Griffies, S. M., 2009: Elements of MOM4p1. GFDL Ocean Group Tech. Rep. 6, 444 pp.

Haine, T. W. N., and Coauthors, 2015: Arctic freshwater export: Status, mechanisms, and prospects. *Global Planet. Change*, **125**, 13–35, https://doi.org/10.1016/j.gloplacha.2014.11.013.

Hallberg, R., 2003: The ability of large-scale ocean models to accept parameterizations of boundary mixing, and a description of a refined bulk mixed-layer model. *Near-Boundary Processes and Their Parameterization: Proc. 2003 'Aha Huliko 'a Hawaiian Winter Workshop*, Honolulu, HI, University of Hawai'i at Mānoa, 187–203, http://www.soest.hawaii.edu/PubServices/2003pdfs/Hallberg.pdf.

——, and A. Adcroft, 2009: Reconciling estimates of the free surface height in Lagrangian vertical coordinate ocean models with mode-split time stepping. *Ocean Modell.*, **29**, 15–26, https://doi.org/10.1016/j.ocemod.2009.02.008.

Hátún, H., C. C. Eriksen, and P. B. Rhines, 2007: Buoyant eddies entering the Labrador Sea observed with gliders and altimetry. *J. Phys. Oceanogr.*, **37**, 2838–2854, https://doi.org/10.1175/2007JPO3567.1.

Hu, A., and Coauthors, 2012: Role of the Bering Strait on the hysteresis of the ocean conveyor belt circulation and glacial climate stability. *Proc. Natl. Acad. Sci. USA*, **109**, 6417–6422, https://doi.org/10.1073/pnas.1116014109.

——, G. A. Meehl, W. Han, B. Otto-Bliesner, A. Abe-Ouchi, and N. Rosenbloom, 2015: Effects of the Bering Strait closure on AMOC and global climate under different background climates. *Prog. Oceanogr.*, **132**, 174–196, https://doi.org/10.1016/j.pocean.2014.02.004.

Jackson, L. C., R. Kahana, T. Graham, M. A. Ringer, T. Woollings, J. V. Mecking, and R. A. Wood, 2015: Global and European climate impacts of a slowdown of the AMOC in a high resolution GCM. *Climate Dyn.*, **45**, 3299–3316, https://doi.org/10.1007/s00382-015-2540-2.

Johns, W. E., and Coauthors, 2011: Continuous, array-based estimates of Atlantic Ocean heat transport at 26.5°N. *J. Climate*, **24**, 2429–2449, https://doi.org/10.1175/2010JCLI3997.1.

Kawasaki, T., and H. Hasumi, 2014: Effect of freshwater from the West Greenland Current on the winter deep convection in the Labrador Sea. *Ocean Modell.*, **75**, 51–64, https://doi.org/10.1016/j.ocemod.2014.01.003.

Komuro, Y., and H. Hasumi, 2005: Intensification of the Atlantic deep circulation by the Canadian Archipelago throughflow. *J. Phys. Oceanogr.*, **35**, 775–789, https://doi.org/10.1175/JPO2709.1.

Kraus, E. B., and J. S. Turner, 1967: A one-dimensional model of the seasonal thermocline: II. The general theory and its consequences. *Tellus*, **19** (1), 98–106, https://doi.org/10.3402/tellusa.v19i1.9753.

Kuhlbrodt, T., A. Griesel, M. Montoya, A. Levermann, M. Hofmann, and S. Rahmstorf, 2007: On the driving processes of the Atlantic meridional overturning circulation. *Rev. Geophys.*, **45**, RG2001, https://doi.org/10.1029/2004RG000166.

Large, W. G., J. C. McWilliams, and S. C. Doney, 1994: Oceanic vertical mixing: A review and a model with a nonlocal boundary layer parameterization. *Rev. Geophys.*, **32**, 363–404, https://doi.org/10.1029/94RG01872.

Liu, Y., R. Hallberg, O. Sergienko, B. L. Samuels, M. Harrison, and M. Oppenheimer, 2018: Climate response to the meltwater runoff from Greenland ice sheet: Evolving sensitivity to discharging locations. *Climate Dyn.*, https://doi.org/10.1007/s00382-017-3980-7, in press.

Lumpkin, R., and K. Speer, 2007: Global ocean meridional overturning. *J. Phys. Oceanogr.*, **37**, 2550–2562, https://doi.org/10.1175/JPO3130.1.

Manabe, S., and R. J. Stouffer, 1995: Simulation of abrupt climate change induced by freshwater input to the North Atlantic Ocean. *Nature*, **378**, 165–167, https://doi.org/10.1038/378165a0.

Marnela, M., B. Rudels, I. Goszczko, A. Beszczynska-Möller, and U. Schauer, 2016: Fram Strait and Greenland Sea transports, water masses, and water mass transformations 1999–2010 (and beyond). *J. Geophys. Res. Oceans*, **121**, 2314–2346, https://doi.org/10.1002/2015JC011312.

Marshall, J., and F. Schott, 1999: Open-ocean convection: Observations, theory, and models. *Rev. Geophys.*, **37**, 1–64, https://doi.org/10.1029/98RG02739.

McGeehan, T., and W. Maslowski, 2011: Impact of shelf–basin freshwater transport on deep convection in the western Labrador Sea. *J. Phys. Oceanogr.*, **41**, 2187–2210, https://doi.org/10.1175/JPO-D-11-01.1.

Melling, H., and Coauthors, 2008: Fresh-water fluxes via Pacific and Arctic outflows across the Canadian polar shelf. *Arctic–Subarctic Ocean Fluxes*, R. R. Dickson et al., Eds., Springer, 193–247.

Münchow, A., H. Melling, and K. K. Falkner, 2006: An observational estimate of volume and freshwater flux leaving the Arctic Ocean through Nares Strait. *J. Phys. Oceanogr.*, **36**, 2025–2041, https://doi.org/10.1175/JPO2962.1.

Myers, P. G., 2005: Impact of freshwater from the Canadian Arctic Archipelago on Labrador Sea water formation. *Geophys. Res. Lett.*, **32**, L06605, https://doi.org/10.1029/2004GL022082.

——, C. Donnelly, and M. H. Ribergaard, 2009: Structure and variability of the West Greenland Current in summer derived from 6 repeat standard sections. *Prog. Oceanogr.*, **80**, 93–112, https://doi.org/10.1016/j.pocean.2008.12.003.

Otto-Bliesner, B. L., A. Jahn, R. Feng, E. C. Brady, A. Hu, and M. Löfverström, 2017: Amplified North Atlantic warming in the late Pliocene by changes in Arctic gateways. *Geophys. Res. Lett.*, **44**, 957–964, https://doi.org/10.1002/2016GL071805.

Peterson, I., J. Hamilton, S. Prinsenberg, and R. Pettipas, 2012: Wind-forcing of volume transport through Lancaster Sound.

J. Geophys. Res., **117**, C11018, https://doi.org/10.1029/2012JC008140.

Pickart, R. S., and M. A. Spall, 2007: Impact of Labrador Sea convection on the North Atlantic meridional overturning circulation. *J. Phys. Oceanogr.*, **37**, 2207–2227, https://doi.org/10.1175/JPO3178.1.

Prinsenberg, S., and J. Hamilton, 2005: Monitoring the volume, freshwater and heat fluxes passing through Lancaster Sound in the Canadian Arctic Archipelago. *Atmos.–Ocean*, **43**, 1–22, https://doi.org/10.3137/ao.430101.

——, ——, I. Peterson, and R. Pettipas, 2009: Observing and interpreting the seasonal variability of the oceanographic fluxes passing through Lancaster Sound of the Canadian Arctic Archipelago. *Influence of Climate Change on the Changing Arctic and Sub-Arctic Conditions*, J. C. J. Nihoul and A. G. Kostianoy, Eds., NATO Science for Peace and Security Series C: Environmental Security, Springer, 125–143.

Roche, D. M., A. P. Wiersma, and H. Renssen, 2010: A systematic study of the impact of freshwater pulses with respect to different geographical locations. *Climate Dyn.*, **34**, 997–1013, https://doi.org/10.1007/s00382-009-0578-8.

Saenko, O. A., A. J. Weaver, D. Y. Robitaille, and G. M. Flato, 2007: Warming of the subpolar Atlantic triggered by freshwater discharge at the continental boundary. *Geophys. Res. Lett.*, **34**, L15604, https://doi.org/10.1029/2007GL030674.

——, F. Dupont, D. Yang, P. G. Myers, I. Yashayaev, and G. C. Smith, 2014: Role of resolved and parameterized eddies in the Labrador Sea balance of heat and buoyancy. *J. Phys. Oceanogr.*, **44**, 3008–3032, https://doi.org/10.1175/JPO-D-14-0041.1.

Schmidt, S., and U. Send, 2007: Origin and composition of seasonal Labrador Sea freshwater. *J. Phys. Oceanogr.*, **37**, 1445–1454, https://doi.org/10.1175/JPO3065.1.

Smith, R. S., and J. M. Gregory, 2009: A study of the sensitivity of ocean overturning circulation and climate to freshwater input in different regions of the North Atlantic. *Geophys. Res. Lett.*, **36**, L15701, https://doi.org/10.1029/2009GL038607.

Spence, J. P., M. Eby, and A. J. Weaver, 2008: The sensitivity of the Atlantic meridional overturning circulation to freshwater forcing at eddy-permitting resolutions. *J. Climate*, **21**, 2697–2710, https://doi.org/10.1175/2007JCLI2103.1.

Stouffer, R. J., and Coauthors, 2006: Investigating the causes of the response of the thermohaline circulation to past and future climate changes. *J. Climate*, **19**, 1365–1387, https://doi.org/10.1175/JCLI3689.1.

Talley, L. D., 2008: Freshwater transport estimates and the global overturning circulation: Shallow, deep and throughflow components. *Prog. Oceanogr.*, **78**, 257–303, https://doi.org/10.1016/j.pocean.2008.05.001.

——, J. L. Reid, and P. E. Robbins, 2003: Data-based meridional overturning streamfunctions for the global ocean. *J. Climate*, **16**, 3213–3226, https://doi.org/10.1175/1520-0442(2003)016<3213:DMOSFT>2.0.CO;2.

Våge, K., and Coauthors, 2011: The Irminger Gyre: Circulation, convection, and interannual variability. *Deep-Sea Res. I*, **58**, 590–614, https://doi.org/10.1016/j.dsr.2011.03.001.

Velicogna, I., T. C. Sutterley, and M. R. Van Den Broeke, 2014: Regional acceleration in ice mass loss from Greenland and Antarctica using GRACE time-variable gravity data. *Geophys. Res. Lett.*, **41**, 8130–8137, https://doi.org/10.1002/2014GL061052.

Wadley, M. R., and G. R. Bigg, 2002: Impact of flow through the Canadian Archipelago and Bering Strait on the North Atlantic and Arctic circulation: An ocean modelling study. *Quart. J. Roy. Meteor. Soc.*, **128**, 2187–2203, https://doi.org/10.1256/qj.00.35.

Wang, H., S. A. Legg, and R. W. Hallberg, 2015: Representations of the Nordic seas overflows and their large scale climate impact in coupled models. *Ocean Modell.*, **86**, 76–92, https://doi.org/10.1016/j.ocemod.2014.12.005.

Woodgate, R. A., T. J. Weingartner, and R. Lindsay, 2012: Observed increases in Bering Strait oceanic fluxes from the Pacific to the Arctic from 2001 to 2011 and their impacts on the Arctic Ocean water column. *Geophys. Res. Lett.*, **39**, L24603, https://doi.org/10.1029/2012GL054092.

Yang, Q., T. H. Dixon, P. G. Myers, J. Bonin, D. Chambers, M. R. Van Den Broeke, M. H. Ribergaard, and J. Mortensen, 2016: Recent increases in Arctic freshwater flux affects Labrador Sea convection and Atlantic overturning circulation. *Nat. Commun.*, **7**, 10525, https://doi.org/10.1038/ncomms10525.

Yashayaev, I., 2007: Hydrographic changes in the Labrador Sea, 1960–2005. *Prog. Oceanogr.*, **73**, 242–276, https://doi.org/10.1016/j.pocean.2007.04.015.

——, and J. W. Loder, 2017: Further intensification of deep convection in the Labrador Sea in 2016. *Geophys. Res. Lett.*, **44**, 1429–1438, https://doi.org/10.1002/2016GL071668.

Yeager, S., and G. Danabasoglu, 2014: The origins of late-twentieth-century variations in the large-scale North Atlantic circulation. *J. Climate*, **27**, 3222–3247, https://doi.org/10.1175/JCLI-D-13-00125.1.